Robust method for identifying material parameters based on virtual fields in elastodynamics

Clément Touzeau, Benoit Magnain, Gilles Lubineau, Éric Florentin

Version of Record: https://www.sciencedirect.com/science/article/pii/S0898122118304231
Manuscript_6ad14690c3027466100f038b3c2249ef

Robust method for identifying material parameters based on virtual fields in elastodynamics

Clément Touzeau[a], Benoît Magnain[a], Gilles Lubineau[b], Eric Florentin[a,*]

[a] *INSA CVL, Univ. Orléans, Univ. Tours, LaMé, F-18022 Bourges, France.*
[b] *King Abdullah University of Science and Technology (KAUST), Physical Science and Engineering Division (PSE), COHMAS Laboratory, Thuwal 23955-6900, Saudi Arabia*

Abstract

We develop an inverse method with the purpose of extracting elastic properties of materials in the framework of transient dynamics. To this end, we create a small linear system based on a set of well-chosen time-dependent virtual fields (VF) and measurement data. The parameters are the solutions of this system and can be quickly extracted. We compare this new method with the classical finite element model updating (FEMU) method for different case studies. In our study, the measurements are synthetic, *i.e*, they are calculated using a fine finite element (FE) model. Uniform white noise is added to model measurement uncertainties. Results, based on Monte Carlo simulations, show that our method is more robust and accurate than the FEMU method for an acceptable noise level. Our new method appears well-adapted to linear elasticity in transient dynamics.

Keywords: Robust identification; time-dependent virtual fields; transient dynamics; linear elasticity.

1. Introduction

Progress in mechanical engineering and image processing has led to the continuous development of contact-less full-field measurement techniques such as the digital image correlation (DIC)[18, 7]. Inverse methods using information provided by the DIC technique have been created to characterize materials by identifying the parameters governing the constitutive law of a given material. The identification process of material parameters can be especially challenging in transient dynamics, due to the important flow of registered data. In this paper, we propose a new, multi-step, identification method for extracting elastic properties of materials in a transient state.

This new method, based on a variational formulation in transient dynamics, introduces a particular set of virtual fields that leads to a linear system of equations. Solving the system allow us to directly extract the material elastic properties.

*corresponding author, email: eric.florentin@insa-cvl.fr

This last step, as well as the absence of any finite element resolution during the extraction of the parameters, are two key characteristics of our proposed method. The use of virtual fields for identification purposes has been investigated by Grédiac et al., by applying the virtual field method (VFM) to numerous configurations [13, 14]. The FEMU method [15] is more intuitive than the VFM but requires an iterative procedure involving costly finite element resolution to extract its constitutive parameters. FEMU is based on the minimisation of a cost function measuring the gap between one measure (usually obtain by DIC) and several finite element resolutions. It is common to create the cost function by using the least square error between a measured displacement field and the displacement calculated by finite element simulations [17]. Another approach for constructing the cost function with geometric quantities was recently presented by Touzeau et al., in [20]. In their study, the authors report interesting results in the framework of large transformations. The constitutive equation gap method (CEGM) [11, 12, 10] and the equilibrium gap method (EGM) [8] are two examples of other methods based on the minimization of a cost function. Various popular identification strategies can be found in the scientific literature, including review articles by Bonnet and Constantinescu [5] or Avril et al. [2] for the case of linear elasticity. Other method, also based on the choice of special fields, such as the reciprocity gap method (RGM) can be used for material parameters identification purposes. An example for elastodynamics studies is given in [6].

Our proposed method is assessed by comparison with the classical finite element model updating (FEMU) method [15]. Our data are synthetic, and built using a refined finite element simulation. In order to take into account imperfections inherent to the practical use of the method, perturbations are introduced. We generate the synthetic data starting from the exact value of material parameters which are known, this makes it possible to measure the identification error at the end of the identification process. A probabilistic study is performed by operating a Monte Carlo simulation on several test case configurations. Both noise on measurements and uncertainties on the loading conditions are considered, as done in many other studies [9, 19, 16, 1]. During our numerical investigations, methods are evaluated in accuracy, robustness and CPU time consuming.

2. Problem framework

In this section, we present the notations and the equations of the direct problem used in the identification procedure and provide a concise description of the finite element resolution. We also describe the build of the synthetic displacement field used for the numerical investigations. Finally, we give an overview of the FEMU method used for comparison of accuracy and robustness.

2.1. Continuous problem in transient dynamics

The direct problem deals with the theory of continuum mechanics in transient dynamics under the assumption of small perturbations and plane stress state in linear elasticity. Here, we present the general

statement of the direct problem in 2D. We consider a solid as a closed subspace of $\mathbb{R}^2$, denoted Ω, as shown in Figure 1. We study the mechanical behaviour of this solid for the time interval $\tau = [0, t_f]$.

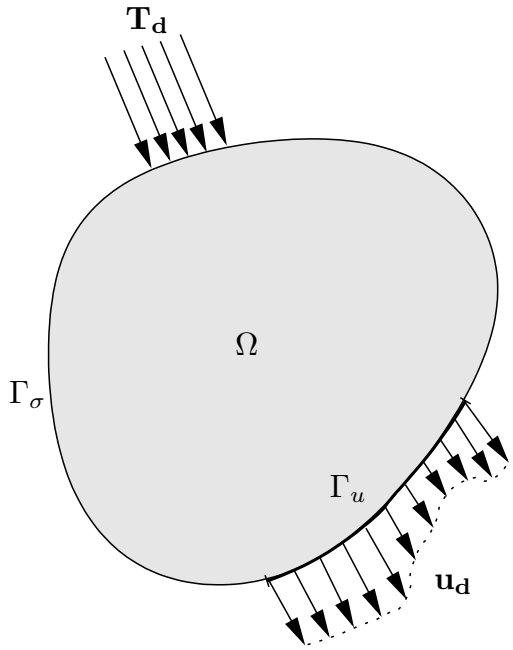

Figure 1: Continuous problem

The partition of its boundary $\partial\Omega$ can be defined as follows:

$$\begin{aligned} \Gamma_\sigma \cup \Gamma_u &= \partial\Omega, \\ \Gamma_\sigma \cap \Gamma_u &= \emptyset. \end{aligned} \tag{1}$$

where the tractions $\boldsymbol{T}_d$ are defined on Γ_σ and the displacements $\boldsymbol{u}_d$ are imposed on Γ_u. The body forces are neglected and no contact occurs during the study. The problem consists of finding the displacement $\boldsymbol{u}(\boldsymbol{x}, t)$ by knowing the geometry, the boundary conditions and the material constitutive law. The solution is unique and the governing equations are:

$$div\,[2\mu\boldsymbol{\epsilon} + \lambda tr(\boldsymbol{\epsilon})\mathbb{I}] = \rho\ddot{\boldsymbol{u}} \quad \text{in} \quad \Omega \times \tau \tag{2}$$

$$[2\mu\boldsymbol{\epsilon} + \lambda tr(\boldsymbol{\epsilon})\mathbb{I}]\,.\,\boldsymbol{n} = \boldsymbol{T}_d \quad \text{on} \quad \Gamma_\sigma \times \tau \tag{3}$$

$$\boldsymbol{u}_d = \boldsymbol{0} \quad \text{on} \quad \Gamma_u \times \tau \tag{4}$$

$$\boldsymbol{\epsilon} = \frac{1}{2}(\nabla\,\boldsymbol{u} + \nabla^T\,\boldsymbol{u}) \quad \text{in} \quad \Omega \times \tau \tag{5}$$

$$\boldsymbol{u}|_{t=0} = 0 \quad \text{and} \quad \dot{\boldsymbol{u}}|_{t=0} = 0 \quad \text{in} \quad \Omega \tag{6}$$

In this equation system, all the fields depend on space and time, but for the sake of clarity, we do not make this appear in the notations. We define $\boldsymbol{\theta} = (\lambda, \mu)^T$ as the set of Lamé parameters representing the

elastic properties of the constitutive material. ρ represent the density of the constitutive material, $\boldsymbol{\epsilon}$ the linearised strain tensor, $\ddot{\boldsymbol{u}}$ the acceleration term of the solution, $\mathbb{I}$ the matrix identity and $\boldsymbol{n}$ the normal vector to Γ_σ. Finally, the initial conditions are defined by equation (6).

2.2. Finite element analysis

In order to resolve the system of equations introduced in Section 2.1, we perform a finite element analysis and use a classical space discretization:

$$\boldsymbol{u}(\boldsymbol{x},t) = \sum_{i=1}^{N_{FE}} \boldsymbol{u}_i(t) N_i(\boldsymbol{x}) \tag{7}$$

where $\boldsymbol{u}_i(t)$ are the vector of nodal displacements and $N_i(\boldsymbol{x})$, $i = 1, 2, \ldots, N_{FE}$ are the finite elements shape functions associated to the mesh of Ω.

The global vector of unknowns $\boldsymbol{U}(t) = [\boldsymbol{u}_1(t)^T\ \boldsymbol{u}_2(t)^T\ \ldots\ \boldsymbol{u}_{N_{FE}}(t)^T]^T$ is the solution to the equation:

$$\mathbb{M}\ddot{\boldsymbol{U}}(t) + \mathbb{K}(\boldsymbol{\theta})\boldsymbol{U}(t) = \boldsymbol{F}(t) \qquad \forall\, t \in \tau \tag{8}$$

where $\mathbb{M}$ is the mass matrix, $\mathbb{K}(\boldsymbol{\theta})$ the rigidity matrix and $\boldsymbol{F}(t)$ the external forces vector.

In order to solve equation (8), we perform a time discretization of the time interval τ:

$$t_n = n\Delta t \quad \text{with} \quad n \in [0, N_{meas}] \quad \text{and} \quad N_{meas} = \frac{t_f}{\Delta t} \tag{9}$$

with N_{meas} the number of records made during the experimental procedure. In the following, the term $\boldsymbol{U}(t_n)$ is simply denoted $\boldsymbol{U}_n$. We then solve the equation (8) using the well-known Newmark scheme by making the following assumptions:

$$\dot{\boldsymbol{U}}_{n+1} = \dot{\boldsymbol{U}}_n + \Delta t \left((1-\gamma)\ddot{\boldsymbol{U}}_n + \gamma \ddot{\boldsymbol{U}}_{n+1} \right) \tag{10}$$

$$\boldsymbol{U}_{n+1} = \boldsymbol{U}_n + \Delta t \dot{\boldsymbol{U}}_n + (\Delta t)^2 \left((\frac{1}{2} - \beta)\ddot{\boldsymbol{U}}_n + \beta \ddot{\boldsymbol{U}}_{n+1} \right) \tag{11}$$

where β and γ are the parameters of the scheme. By choosing the classical set of values 0.25 for β and 0.5 for γ, we obtain an implicit scheme called *the average acceleration method*. In the case of linear elasticity, this scheme is of the second order of accuracy and is unconditionally stable.

Using equation (8) at the time step $n+1$ with (10) and (11), one can write:

$$\tilde{\mathbb{K}}(\boldsymbol{\theta})\boldsymbol{U}_{n+1} = \tilde{\boldsymbol{F}}_{n+1} \tag{12}$$

with:

$$\tilde{\mathbb{K}}(\boldsymbol{\theta}) = \mathbb{K}(\boldsymbol{\theta}) + \frac{1}{\beta \Delta t^2}\mathbb{M} \tag{13}$$

and:

$$\tilde{\boldsymbol{F}}_{n+1} = \boldsymbol{F}_{n+1} + \mathbb{M}\Big(\frac{1}{\beta\Delta t^2}\boldsymbol{U}_n + \frac{1}{\beta\Delta t}\dot{\boldsymbol{U}}_n + (\frac{1}{2\beta} - 1)\ddot{\boldsymbol{U}}_n\Big) \tag{14}$$

Starting from the initial conditions at $t = 0$ (equation (6)), the linear system in equation (12) can be solved iteratively to obtain the displacement for all time steps.

2.3. Building the synthetic data

In order to validate the proposed identification method, the measured displacement field $\boldsymbol{U}(t)$ is replaced by synthetic data. First, a refined solution to the direct problem is computed with the exact values of Lamé parameters ($\boldsymbol{\theta}_{ex}$). Indeed, the Newmark scheme is performed using a very small time steps Δt combined with a very fine mesh. For each time steps, the solution is stored on a measurement grid, denoted $\boldsymbol{U}_n^{ref}$. Thus, $\boldsymbol{U}_n^{ref}$ (for all n in $[1, N_{meas}]$) constitutes the reference for our measurements. These synthetic data are interesting because they make it possible to estimate the quality of the identification procedure.

The displacement vectors $\boldsymbol{U}_n^{ref}$ of size N_{eq} (the number of equations), $\forall\, n \in [1, N_{meas}]$ are gathered into a matrix $\mathbb{U}^{ref}$:

$$\mathbb{U}^{ref} = \Big[\boldsymbol{U}_1^{ref}, ..., \boldsymbol{U}_{N_{meas}}^{ref}\Big] \tag{15}$$

We consider the displacement matrix $\mathbb{U}^{ref}$ to be exact, and the error due to the finite element is neglected. In reality, experimental set-ups and image processing always provide a measured displacement field with perturbations. Noise can be created because of the quality of the CCD sensors, the experimental benchmark and/or the user (see [4] for more details). In a small perturbation framework, the signal-to-noise ratio is low and the noise perturbation cannot be ignored in the study.

In our study, we choose to add noise synthetically by considering a random perturbation (*i.e.* uniform white noise) and use a Monte-Carlo process to study the robustness of the proposed method. The randomness is characterized by the parameter ω, with $\omega_p,\ p \in \{1, 2, ..., N_{MC}\}$ the N_{MC} Monte Carlo realizations. The number of Monte-Carlo realizations must be large to obtain a good accuracy of the Monte-Carlo analysis; therefore, we use $N_{MC} = 10^4$ in our study. The new displacement field $\mathbb{U}^{meas}$, considered as more realistic, is build from $\mathbb{U}^{ref}$ as follows:

$$\mathbb{U}^{meas}(\omega) = \mathbb{U}^{ref} + \delta\mathbb{U}(\omega) \tag{16}$$

The perturbation matrix $\delta\mathbb{U}(\omega)$ is a proportional white noise perturbation. Each component δU_{ij} of matrix $\delta\mathbb{U}(\omega)$ is expressed as follows:

$$\delta U_{ij}(\omega) = \alpha\psi_{ij}(\omega)U_{ij}^{ref} \tag{17}$$

where $\psi_{ij}(\omega)$ is a $N_{meas} \times N_{eq}$ uniform random variable-centered on zero with values within the range $[-1, 1]$. α is a scalar parameter characterizing the magnitude of the white noise.

N_{MC} Monte Carlo realizations $\mathbb{U}^{meas}(\omega_p)$ ($p \in \{1, 2, ..., N_{MC}\}$) of the random matrix $\mathbb{U}^{meas}(\omega)$ can easily be constructed for the Monte-Carlo analysis.

2.4. Reference identification method

The accuracy and the robustness of our proposed method, is assessed by comparison with the FEMU method [15],[17], a popular, established method for extracting constitutive parameters that can easily be extended to transient dynamics. This method aims at minimizing a cost function that describes the distance between the measured field and a calculated field obtained by using the finite element method:

$$\boldsymbol{\theta}_{id}(\omega) = \underset{\boldsymbol{\theta}}{\operatorname{argmin}}\, C(\boldsymbol{\theta}, \omega) \tag{18}$$

In equation (18), $\boldsymbol{\theta}_{id}(\omega)$ is a random vector due to the random perturbation $\delta\mathbb{U}(\omega)$ associated to the measured displacements. The displacement vectors $\boldsymbol{U}_n^{calc}$ of size N_{eq} (the number of equations), $\forall n \in [1, N_{meas}]$ are gathered into a matrix $\mathbb{U}^{calc}$. We introduce the cost function $C_{\mathbf{u}}(\boldsymbol{\theta}, \omega)$ as follows:

$$C_{\mathbf{u}}(\boldsymbol{\theta}, \omega) = \sum_{i}^{N_{meas}} \sum_{j}^{N_{eq}} \left(U_{ij}^{meas}(\omega) - U_{ij}^{calc}(\boldsymbol{\theta}) \right)^2 \tag{19}$$

where U_{ij}^{calc} are the components of matrix $\mathbb{U}^{calc}$.

Because of the large number of simulations needed to minimize each realizations $C_{\mathbf{u}}(\boldsymbol{\theta}, \omega_p)$ ($p \in \{1, 2, ..., N_{MC}\}$) of the random variable $C_{\mathbf{u}}(\boldsymbol{\theta}, \omega)$, we use a centered difference scheme with a lumped mass matrix, instead of the Newmark scheme, to calculate $\boldsymbol{U}_n^{calc}$. Similarly, a coarser mesh is built for the reference solution. Finally, the time step Δt is chosen with respect to the Courant-Friedricks-Levy condition:

$$\Delta t \leq \Delta t_{cr} = \frac{l}{c} \tag{20}$$

where c is the wave celerity in the material and l is the critic length of the smallest element of the mesh. This scheme is selected because it does not need a system resolution since the mass matrices are lumped.

3. Developed identification strategy

Here, we propose an inverse method for extracting the constitutive parameters of the material directly, without any finite element resolutions. This makes it different from the FEMU method, which needs iterative resolutions during the minimization process. In the following equations, the random displacement $\boldsymbol{U}^{meas}(t, \omega)$ is simply denoted $\boldsymbol{U}$.

3.1. General principle for extracting two parameters

The linear elasticity of the material is expressed using a stiffness matrix $\mathbb{K}(\boldsymbol{\theta})$ and the Lamé coefficients λ and μ:

$$\mathbb{K}(\boldsymbol{\theta}) = \lambda\mathbb{K}_{\lambda} + \mu\mathbb{K}_{\mu} \tag{21}$$

where $\mathbb{K}_\lambda$ and $\mathbb{K}_\mu$ are symmetric definite positive matrices.

Using equation (21), one can rewrite equation (8) as follows:

$$\mathbb{M}\ddot{\boldsymbol{U}} + (\lambda\mathbb{K}_\lambda + \mu\mathbb{K}_\mu)\boldsymbol{U} = \boldsymbol{F} \qquad \forall\, t \in [0, t_f] \tag{22}$$

The first idea of the method consists in writing a variational formulation of the problem defined in equation (22). $\boldsymbol{U}^*(t)$ (denoted $\boldsymbol{U}^*$ in the following) is introduced as a virtual field defined over $[0, t_f]$. $\boldsymbol{U}^*$ is selected according to the Dirichlet conditions; it is continuous for the whole domain Ω (kinematic admissibility). Therefore:

$$\int_0^{t_f} \left(\mathbb{M}\ddot{\boldsymbol{U}} + (\lambda\mathbb{K}_\lambda + \mu\mathbb{K}_\mu)\boldsymbol{U} - \boldsymbol{F}\right)^T \boldsymbol{U}^*\, dt = 0 \tag{23}$$

or, after some simple operations:

$$\int_0^{t_f} \ddot{\boldsymbol{U}}^T \mathbb{M}\boldsymbol{U}^*\, dt + \int_0^{t_f} \boldsymbol{U}^T\big(\lambda\mathbb{K}_\lambda + \mu\mathbb{K}_\mu\big)\boldsymbol{U}^*\, dt - \int_0^{t_f} \boldsymbol{F}^T\boldsymbol{U}^*\, dt = 0 \tag{24}$$

In equation (24), the first term is of great importance as it provides an expression of the acceleration field, $\ddot{\boldsymbol{U}}$, in terms of the measured data. $\ddot{\boldsymbol{U}}$ is computed from the measured displacement field using two temporal derivations. This step can lead to major errors due to noise in the measured data. To address this issue, we perform two successive partial integrations, which leads to the following equations:

$$\int_0^{t_f} \boldsymbol{U}^T\mathbb{M}\ddot{\boldsymbol{U}}^* dt + \int_0^{t_f} \boldsymbol{U}^T\big(\lambda\mathbb{K}_\lambda + \mu\mathbb{K}_\mu\big)\boldsymbol{U}^* dt - \int_0^{t_f} \boldsymbol{F}^T\boldsymbol{U}^* dt + \big[\dot{\boldsymbol{U}}^T\mathbb{M}\boldsymbol{U}^*\big]_0^{t_f} - \big[\boldsymbol{U}^T\mathbb{M}\dot{\boldsymbol{U}}^*\big]_0^{t_f} = 0 \tag{25}$$

The main advantage of this new formulation is that it only requires knowledge of the measured displacement field over the time and the measured velocity field at t_0 and at t_f.

$\ddot{\boldsymbol{U}}^*$ must be chosen derivable twice over time. In this paper, we propose to study the following set of virtual fields:

$$\begin{cases} \boldsymbol{U}_1^* = \boldsymbol{U} \quad \forall t \in [0, t_f] \\ \boldsymbol{U}_{i+2}^* = t^i\mathbf{1} \quad \forall t \in [0, t_f] \quad i \in \mathbb{N} \end{cases} \tag{26}$$

where vector $\mathbf{1}$ represents a vector filled with ones $(1, 1)^T$.

$\boldsymbol{U}_1^*$, corresponds to the measured displacement field. The second order differentiation $\ddot{\boldsymbol{U}}^* = \ddot{\boldsymbol{U}}_1^*$ cannot be performed using a basic differentiation. Indeed, due to noise propagation, it is very challenging to estimate it properly. A specific algorithm has been used and is presented in section 3.3.3. For $\boldsymbol{U}_{i+2}^*, (i \in \mathbb{N})$ the dependency with t is analytical, which conduce to an analytical expression of the second order derivative : $\ddot{\boldsymbol{U}}^* = \ddot{\boldsymbol{U}}_{2+i}^*$.

In order to identify the two Lamé coefficients, we choose two virtual fields and build the linear system with two equations and two unknowns. We propose to use the first two virtual fields of the set: $\boldsymbol{U}_1^*$ and $\boldsymbol{U}_2^*$.

Thus, we obtain:

$$\begin{cases} \lambda \int_0^{t_f} \boldsymbol{U}^T \mathbb{K}_\lambda \boldsymbol{U} dt + \mu \int_0^{t_f} \boldsymbol{U}^T \mathbb{K}_\mu \boldsymbol{U} dt = \int_0^{t_f} \boldsymbol{F}^T \boldsymbol{U} dt - \left[\dot{\boldsymbol{U}}^T \mathbb{M} \boldsymbol{U}\right]_0^{t_f} + \left[\boldsymbol{U}^T \mathbb{M} \dot{\boldsymbol{U}}\right]_0^{t_f} - \int_0^{t_f} \boldsymbol{U}^T \mathbb{M} \ddot{\boldsymbol{U}} dt \\ \lambda \int_0^{t_f} \boldsymbol{U}^T \mathbb{K}_\lambda t^0 \mathbf{1} dt + \mu \int_0^{t_f} \boldsymbol{U}^T \mathbb{K}_\mu t^0 \mathbf{1} dt = \int_0^{t_f} \boldsymbol{F}^T t^0 \mathbf{1} dt - \left[\dot{\boldsymbol{U}}^T \mathbb{M} t^0 \mathbf{1}\right]_0^{t_f} \end{cases} \tag{27}$$

The system (27) can be rewritten as follows:

$$A_{ij} \theta_j = b_i \tag{28}$$

with:

$$A_{11} = \int_0^{t_f} \boldsymbol{U}^T \mathbb{K}_\lambda \boldsymbol{U} \, dt \tag{29}$$

$$A_{12} = \int_0^{t_f} \boldsymbol{U}^T \mathbb{K}_\mu \boldsymbol{U} \, dt \tag{30}$$

$$A_{21} = \int_0^{t_f} \boldsymbol{U}^T \mathbb{K}_\lambda t^0 \mathbf{1} \, dt \tag{31}$$

$$A_{22} = \int_0^{t_f} \boldsymbol{U}^T \mathbb{K}_\mu t^0 \mathbf{1} \, dt \tag{32}$$

$$b_1 = \int_0^{t_f} \boldsymbol{F}^T \boldsymbol{U} \, dt + \left[\boldsymbol{U}^T \mathbb{M} \dot{\boldsymbol{U}}\right]_0^{t_f} - \left[\dot{\boldsymbol{U}}^T \mathbb{M} \boldsymbol{U}\right]_0^{t_f} - \int_0^{t_f} \boldsymbol{U}^T \mathbb{M} \ddot{\boldsymbol{U}} \, dt \tag{33}$$

$$b_2 = \int_0^{t_f} \boldsymbol{F}^T t^0 \mathbf{1} dt - \left[\dot{\boldsymbol{U}}^T \mathbb{M} t^0 \mathbf{1}\right]_0^{t_f} \tag{34}$$

Because the value of the determinant of $\mathbb{A}$ is not equal to zero, a unique solution exists for each realization of ω. The solution $\boldsymbol{\theta}_{id}$ can be expressed as follows:

$$\lambda_{id} = \frac{b_1 A_{22} - b_2 A_{12}}{\det \mathbb{A}} \quad \text{and} \quad \mu_{id} = \frac{A_{11} b_2 - A_{21} b_1}{\det \mathbb{A}} \tag{35}$$

The unfortunate case, $\det(\mathbb{A}) = 0$, is likely to occur if we introduce a virtual field that conduces to a linear combination of previous equations. A simple manner to avoid this problem is to skip this field and take the next one in the proposed family.

3.2. Extension of the method

Here, we present an extension of the proposed method for an arbitrary number of parameters (*e.g.* orthotropic or heterogeneous material). If n is the amount of material parameters to extract so that $\boldsymbol{\theta} = (\theta_1, \theta_2, ..., \theta_n)^T$, the stiffness matrix $\mathbb{K}(\boldsymbol{\theta})$ must be expressed as:

$$\mathbb{K}(\boldsymbol{\theta}) = \theta_1 \mathbb{K}_{\theta_1} + \theta_2 \mathbb{K}_{\theta_2} + ... + \theta_n \mathbb{K}_{\theta_n} \tag{36}$$

By using as much virtual fields as needed (n), we can establish a linear system of virtual fields as follows:

$$\begin{cases} \theta_1 \int_0^{t_f} \boldsymbol{U}^T \mathbb{K}_{\theta_1} \boldsymbol{U} dt + ... + \theta_n \int_0^{t_f} \boldsymbol{U}^T \mathbb{K}_{\theta_n} \boldsymbol{U} dt = \int_0^{t_f} \boldsymbol{F}^T \boldsymbol{U} dt - \left[\dot{\boldsymbol{U}}^T \mathbb{M} \boldsymbol{U}\right]_0^{t_f} + \left[\boldsymbol{U}^T \mathbb{M} \dot{\boldsymbol{U}}\right]_0^{t_f} - \int_0^{t_f} \boldsymbol{U}^T \mathbb{M} \ddot{\boldsymbol{U}} dt \\ \theta_1 \int_0^{t_f} \boldsymbol{U}^T \mathbb{K}_{\theta_1} t^0 \mathbf{1} dt + ... + \theta_n \int_0^{t_f} \boldsymbol{U}^T \mathbb{K}_{\theta_n} t^0 \mathbf{1} dt = \int_0^{t_f} \boldsymbol{F}^T t^0 \mathbf{1} dt - \left[\dot{\boldsymbol{U}}^T \mathbb{M} t^0 \mathbf{1}\right]_0^{t_f} \\ \theta_1 \int_0^{t_f} \boldsymbol{U}^T \mathbb{K}_{\theta_1} t \mathbf{1}^T dt + ... + \theta_n \int_0^{t_f} \boldsymbol{U}^T \mathbb{K}_{\theta_n} t \mathbf{1}^T dt = \int_0^{t_f} \boldsymbol{F}^T t \mathbf{1}^T dt - \left[\dot{\boldsymbol{U}}^T \mathbb{M} t \mathbf{1}^T\right]_0^{t_f} + \left[\boldsymbol{U}^T \mathbb{M} \mathbb{1} \mathbf{1}^T\right]_0^{t_f} \\ ... \\ \theta_1 \int_0^{t_f} \boldsymbol{U}^T \mathbb{K}_{\theta_1} t^n \mathbf{1}^T dt + ... + \theta_n \int_0^{t_f} \boldsymbol{U}^T \mathbb{K}_{\theta_n} t^n \mathbf{1}^T dt = \int_0^{t_f} \boldsymbol{F}^T t^n \mathbf{1}^T dt - \left[\dot{\boldsymbol{U}}^T \mathbb{M} t^n \mathbf{1}^T\right]_0^{t_f} + \left[\boldsymbol{U}^T \mathbb{M} n t^{n-1} \mathbf{1}^T\right]_0^{t_f} \\ - \int_0^{t_f} \boldsymbol{U}^T \mathbb{M} n(n-1) t^{n-2} \mathbf{1}^T dt \end{cases} \tag{37}$$

or, in matrix form:

$$A_{ij} \theta_j = b_i \tag{38}$$

$\mathbb{A}$ is a n by n square matrix. An analytical resolution can be performed to find the n parameters $\boldsymbol{\theta} = (\theta_1, \theta_2, ..., \theta_n)^T$ as far as n is generally small.

The decomposition described by equation (36) is a limitation. Nevertheless, different extensions remains possible such as orthotropic materials (linear elasticity) or heterogeneous materials like multi-material domain for instance. Such a case will be treated numerically in the section 4.

3.3. Numerical approximations

In our proposed method, we introduce a set of variational formulations of the direct problem. After performing two successive partial integrations, we extract material parameters directly, using a linear system of material parameters. Here, we present the mathematical tools used to calculate the different terms of the matrix $\mathbb{A}$ (see sections 3.1 and 3.2).

3.3.1. Numerical integration

Time integration is performed numerically by using the Simpson scheme. Based on equation (9), we define f as a continuous function on $[0, t_f]$ and $\{y_0, \cdots, y_{N_{meas}}\}$ as the discrete values of the function f. We approximate $\int_0^{t_f} f(t)\, dt$ by:

$$\int_0^{t_f} f(t)\, dt = \frac{\Delta t}{3} \left(y_0 + 4 \sum_{i=0}^{N_{meas}/2} y_{2i+1} + 2 \sum_{i=1}^{N_{meas}/2} y_{2i} + y_{N_{meas}} \right) \tag{39}$$

Where N_{meas} must be an even number. The performed numerical tests shows that the integration error can be neglected in front of the identification error (see equation (43)).

3.3.2. Smoothing of $\boldsymbol{U}_1^*$

In the case of small perturbations, the signal-to-noise ratios are low and the accuracy of the identification method can be limited by measurement uncertainties. Indeed, the time derivation of measured data can lead to major oscillations in calculated terms, which may happen when using $\boldsymbol{U}_1^* = \boldsymbol{U}$ as virtual field. To address this, we propose a numerical approximation that consists of *smoothing* the original data. Using the same notations as in the previous part, the smoothed value, $\tilde{y}_i$, is calculated by:

$$\tilde{y}_i = \frac{y_{i-2\Delta t} + 2y_{i-\Delta t} + 4y_i + 2y_{i+\Delta t} + y_{i+2\Delta t}}{10} \tag{40}$$

One of the advantages of this method is a reduction of the random variation of $\boldsymbol{U}_1^*(t)$ and its derivatives, which means that the signal-to-noise ratios are increased. Our work aims at improving this method in terms of accuracy and robustness, without costing severe additional CPU time computations.

3.3.3. Numerical derivation for $\boldsymbol{U}_1^*$

The second order differentiation for the displacement $\boldsymbol{U}(t)$ is also a delicate part of the procedure. In order to reduce the loss of information due to a bad differentiation approximation, here, we use a numerical model based on a five-point-centered difference scheme to provide an approximation $\dot{f}(t)$ on the time interval $[0, t_f]$. The differentiation term can then be expressed as:

$$\frac{\partial f(t)}{\partial t}\Big|_{t=t_i} = \frac{y_{i-2\Delta t} - 8y_{i-\Delta t} + 8y_{i+\Delta t} - y_{i+2\Delta t}}{12\Delta t} = \dot{y}_i \tag{41}$$

3.4. Evaluation of the identification strategy

Using the previously established values of $\boldsymbol{\theta}_{ex}$ which are used to generate the synthetic measurements, we evaluate the identification error, $\boldsymbol{\epsilon}(\omega)$, a random vector, as the difference between the identified parameters $\boldsymbol{\theta}_{id}(\omega)$ and the exact parameters $\boldsymbol{\theta}_{ex}$:

$$\boldsymbol{\epsilon}(\omega) = \boldsymbol{\theta}_{id}(\omega) - \boldsymbol{\theta}_{ex} \tag{42}$$

Each component of the vector $\boldsymbol{\epsilon}(\omega)$ corresponds to an error on each physical parameters (relative to the corresponding component of $\boldsymbol{\theta}$). Practically, we also define a relative error $\boldsymbol{e}(\omega)$, for each component as:

$$e_i(\omega) = \frac{\epsilon_i}{\theta_{i,ex}} \quad i = \lambda \quad \text{or} \quad \mu \tag{43}$$

The different statistics of $\boldsymbol{e}$ can be obtained by using Monte Carlo simulations. In order to evaluate accuracy and robustness of our proposed method, we define the mean of the relative identification error $\boldsymbol{e}(\omega)$ with $\bar{\boldsymbol{e}}$ expressed as:

$$\bar{\boldsymbol{e}} \approx \frac{1}{N_{MC}} \sum_{p=1}^{N_{MC}} \boldsymbol{e}(\omega_p) \tag{44}$$

Finally, we define the standard deviation of the relative identification error $\boldsymbol{e}(\omega)$ denoted $\hat{\boldsymbol{e}}$ as follows:

$$\hat{\boldsymbol{e}} \approx \sqrt{\frac{1}{N_{MC}} \sum_{p=1}^{N_{MC}} \left(\boldsymbol{e}(\omega_p) - \bar{\boldsymbol{e}}\right)} \tag{45}$$

Using Monte-Carlo simulations, we determinate the discrete Probability Density Function (PDF) and the discrete Cumulative Density Function (CDF). In our work, we focus on the error value $e_i^{90\%}$ that leads to 90 % CDF $CDF(e_i^{90\%}) = 90\%$, meaning that 90% of the realizations $e_i(\omega_p)$ ($p \in \{1, 2, ..., N_{MC}\}$) are below $e_i^{90\%}$.

4. Numerical investigations

Our method is tested for four different systems: one very simple mass-spring system, two systems consisting of 2D squares (with and without a hole) and one system describing a multi-materials domain.

4.1. First case study: mass-spring system

We consider a mass-spring system with a single degree of freedom (see Figure 2). The goal is to identify the stiffness k of the spring using the method presented in section 3. This model provide a numerical benchmark for which an analytical solution is available.

4.1.1. Statement of the problem and data construction

The measured positions are built from the vertical position of the mass m subject to the transient loading, as shown in Figures 2 and 3.

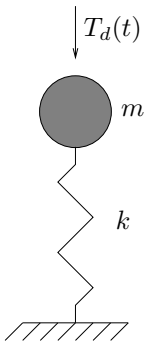

Figure 2: Test case configuration

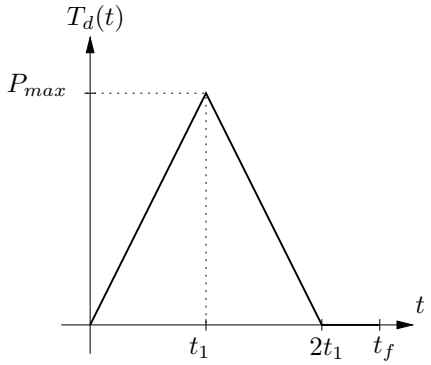

Figure 3: Loading evolution

The measured position of m is denoted $x^{meas}(t, \omega_p)$ and can be expressed as the sum of two terms: the exact part (*e.g.* the analytical solution), denoted $x^{ex}(t)$ and the random perturbation (*e.g.* the measurement error), denoted $\delta x(\omega)$:

$$x^{meas}(t, \omega) = x^{ex}(t) + \alpha\, \psi(\omega)\, x^{ex}(t) \quad \forall t \in [0, t_f] \tag{46}$$

where $\psi(\omega)$ is an uniform random variable centered on zero within $[-1, 1]$.

The first term is a solution of the equilibrium equation:

$$\ddot{x}^{ex}(t) + \frac{k}{m}x^{ex}(t) = \frac{1}{m}T_d(t) \quad \forall t \in [0, t_f] \tag{47}$$

where $\ddot{x}^{ex}(t)$ is the exact acceleration term. The analytical solution for equation (47) is:

$$x^{ex}(t) = \frac{P_{max}}{kt_1}\Big(t - \frac{\sin(\sqrt{\frac{k}{m}}t)}{\sqrt{\frac{k}{m}}}\Big) \quad \forall t \in [0, t_1] \tag{48}$$

$$x^{ex}(t) = \frac{P_{max}}{kt_1}\Big(t - 2t_1 + \frac{2\sin\big(\sqrt{\frac{k}{m}}(t-t_1)\big) - \sin(\sqrt{\frac{k}{m}}t)}{\sqrt{\frac{k}{m}}}\Big) \quad \forall t \in [t_1, 2t_1] \tag{49}$$

$$x^{ex}(t) = \frac{P_{max}}{kt_1}\Big(\frac{2\sin\big(\sqrt{\frac{k}{m}}(t-t_1)\big) + \sin\big(\sqrt{\frac{k}{m}}(2t_1-t)\big) - 1}{\sqrt{\frac{k}{m}}}\Big) \quad \forall t \in [2t_1, t_f] \tag{50}$$

4.1.2. Reference identification method

The minimization problem equation (18) can be simplified for the mass-spring system. It then becomes:

$$k_{id}(\omega) = \underset{k}{\operatorname{argmin}}\, C_x(k, \omega) \tag{51}$$

where $k_{id}(\omega)$ is the identified parameter. The cost function is based on the position evaluation and can be defined by:

$$C_x(k, \omega) = \sum_{i=0}^{N_{meas}} \big(x_i^{meas}(\omega) - x_i^{calc}(k)\big)^2 \tag{52}$$

where $x_i^{meas}(\omega)$ are the measured positions of the mass and $x_i^{calc}(k)$ is the calculated position obtained by using the equation (47) and a Newmark scheme.

4.1.3. Proposed identification method

In this case, the method presented in section 3 can be simplified. The variational formulation of the problem is then written using equation (47) applied to $x^{meas}(t, \omega_p)$:

$$\int_0^{t_f} \Big(\ddot{x}^{meas}(t, \omega_p) + \frac{k}{m}x^{meas}(t, \omega_p) - \frac{1}{m}T_d(t)\Big)x^* \, dt = 0 \tag{53}$$

Where x^* is a virtual position field defined on $[0, t_f]$. The only parameter to extract is then identified by solving one equation:

$$k_{id}(\omega) = \frac{\int_0^{t_f} T_d(t)x^* \, dt - \int_0^{t_f} mx^{meas}(t, \omega)\ddot{x}^* \, dt + [m\dot{x}^* x^{meas}(t, \omega)]_0^{t_f} - [m\dot{x}^{meas}(t, \omega)x^*]_0^{t_f}}{\int_0^{t_f} x^{meas}(t, \omega)x^* \, dt} \tag{54}$$

The same choices can be made for virtual fields:

$$\begin{cases} x_1^* = x^{meas}(t, \omega) & \forall t \in [0, t_f] \\ x_{i+2}^* = t^i & \forall t \in [0, t_f] \quad i \in \mathbb{N} \end{cases} \tag{55}$$

A comparison between several virtual fields leads to the resolution of several equations. Some of them are represented in the following development:

$$\text{for } x_1^* : k_{id}(\omega) = \frac{\int_0^{t_f} T_d(t) x^{meas}\, dt - \int_0^{t_f} m x^{meas} \ddot{x}^{meas}\, dt + [m\dot{x}^{meas} x^{meas}]_0^{t_f} - [m\dot{x}^{meas} x^{meas}]_0^{t_f}}{\int_0^{t_f} \left(x^{meas}\right)^2 dt} \tag{56}$$

$$\text{for } x_{i+2}^* : k_{id}(\omega) = \frac{\int_0^{t_f} T_d(t) t^i\, dt - \int_0^{t_f} m x^{meas} i(i-1) t^{i-2}\, dt + [m i t^{i-1} x^{meas}]_0^{t_f} - [m\dot{x}^{meas} t^i]_0^{t_f}}{\int_0^{t_f} x^{meas} t^i\, dt} \tag{57}$$

The numerical approximations are performed with the mathematical tools defined in the section 3. The identification methods used in our study are listed in Table 1.

4.1.4. Results and discussion

The parameters of the loading evolution are: $t_1 = 1.0\ s$; $t_f = 4.0\ s$ and $P_{max} = 10\ N$. The mass is equal to 30 kg and the stiffness to 745 $N.m^{-1}$. The time step is $\Delta t = 0.1\ s$ so the number of records is $N_{meas} = 40$. The number of Monte Carlo simulations is $N_{MC} = 10^4$. The noise magnitude α varies from 0% to 8% which is considered as coherent for the case of linear elasticity (see [3]).

Table 1: Names of the identification methods used in our study

Name	identification method
m1	$x_2^* = 1$ is used,
m2	$x_3^* = t$ is used,
m3	$x_4^* = t^2$ is used,
m4	$x_1^* = x^{meas}(t,\omega)$ is used,
m5	$x_1^* = x^{meas}(t,\omega)$ is used with a smoothing (equation (40)),
femu	$C_x(k,\omega) = \sum_{i=0}^{N_{meas}} \left(x_i^{meas}(\omega) - x_i^{calc}(k)\right)^2$.

The notation *femu*, used in this part, stand only for the 0D case study. In the other studies (2D studies), the notation FEMU will be used.

As a result of the Monte-Carlo study, Figure 4 shows $e_k^{90\%}$ versus α. Level $e_k^{90\%}$ is defined by $CDF(e_k^{90\%}) = 90\%$. It means that 90% of the realizations $e_k(\omega_p)$ $(p \in \{1, 2, ..., N_{MC}\})$ are below $e_k^{90\%}$.

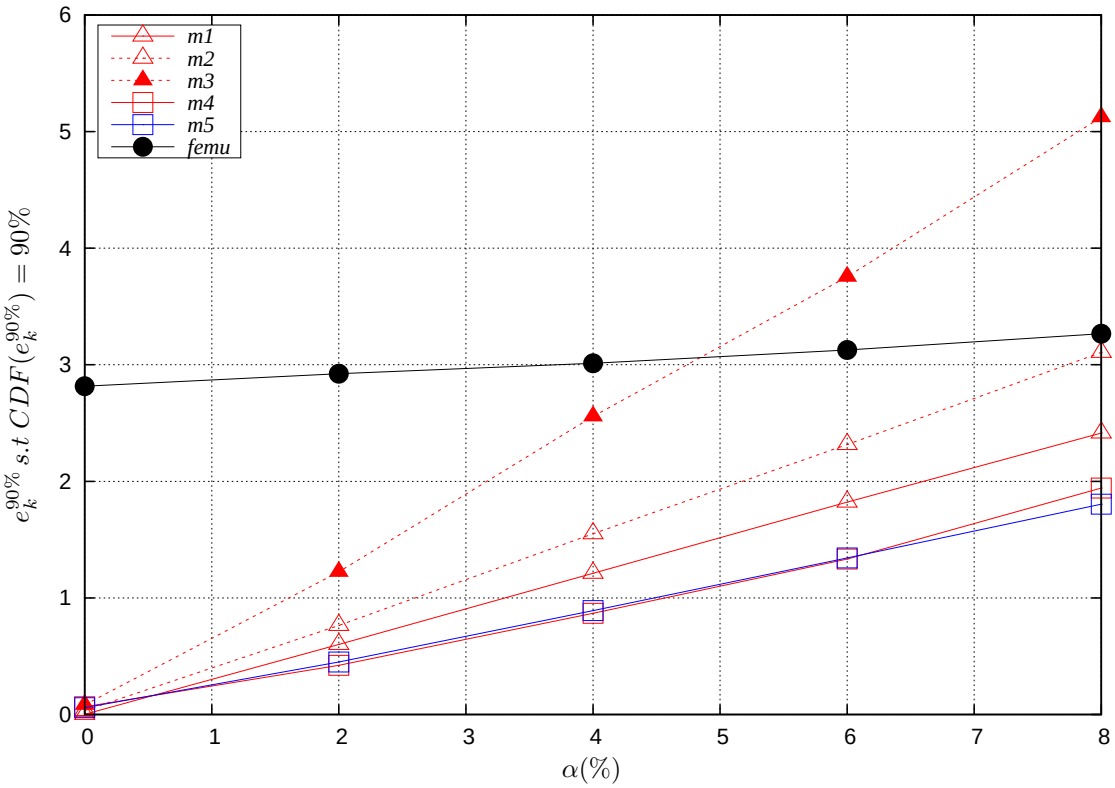

Figure 4: $e_k^{90\%}\ s.t\ CDF(e_k^{90\%}) = 90\%$ vs α

Table 2: $\bar{e}_k$ and $\hat{e}_k$ for different values of α

	α	m1	m2	m3	m4	m5	*femu*
	0%	$1.94e^{-3}$	$3.33e^{-2}$	$8.22e^{-2}$	$6.65e^{-2}$	$5.84e^{-2}$	2.82
	2%	0.31	0.39	0.64	0.22	0.23	2.82
$\bar{e}_k(\%)$	4%	0.62	0.78	1.26	0.45	0.46	2.81
	6%	0.92	1.16	1.89	0.71	0.70	2.82
	8%	1.24	1.55	2.55	1.03	0.92	2.82
	0%	0.00	0.00	0.00	0.00	0.00	0.00
	2%	0.23	0.29	0.47	0.16	0.17	$8.65e^{-2}$
$\hat{e}_k(\%)$	4%	0.46	0.58	0.93	0.33	0.34	0.17
	6%	0.69	0.88	1.42	0.51	0.51	0.27
	8%	0.91	1.17	1.90	0.74	0.68	0.35

Table 2 shows the mean $\bar{e}$ and the standard deviation $\hat{e}$ of $\boldsymbol{e}_k(\omega)$ as a function of α. Results show that, for the most part, virtual fields lead to better results than the *femu* method for reasonable values of noise

amplitude. They also show that although the smoothing technique is not absolutely necessary for such a simple study, it does slightly improve the identification process without inducing any loss of mechanical information. An illustration of this is given in Figure 5 which shows the discrete PDF of the realisation $\boldsymbol{e}_k(\omega_p)$ $(p \in \{1, 2, ..., N_{MC}\})$ associated to Monte-Carlo simulations for $\alpha = 8\%$ and Figure 6, which shows the discrete CDF for the exact same conditions, and so compares the best choice (m5) of the proposed method with *femu*.

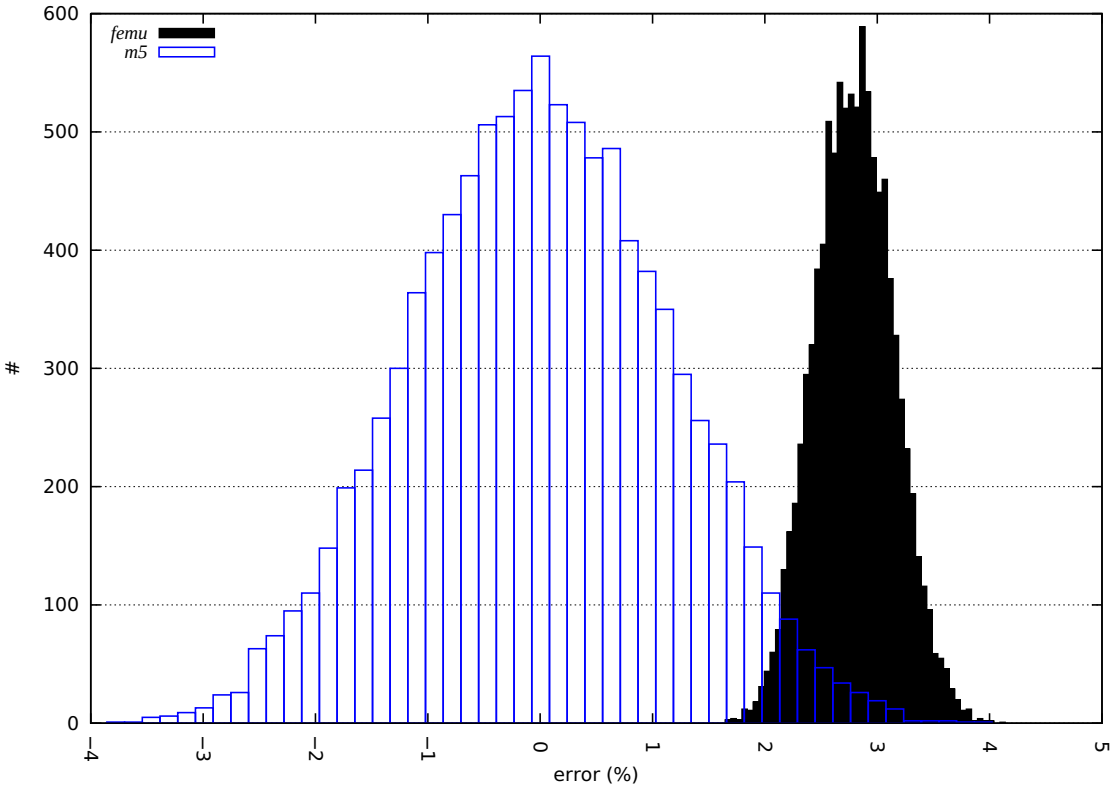

Figure 5: PDF of $\boldsymbol{e}_k$ using m5 (blue) and *femu* (black)

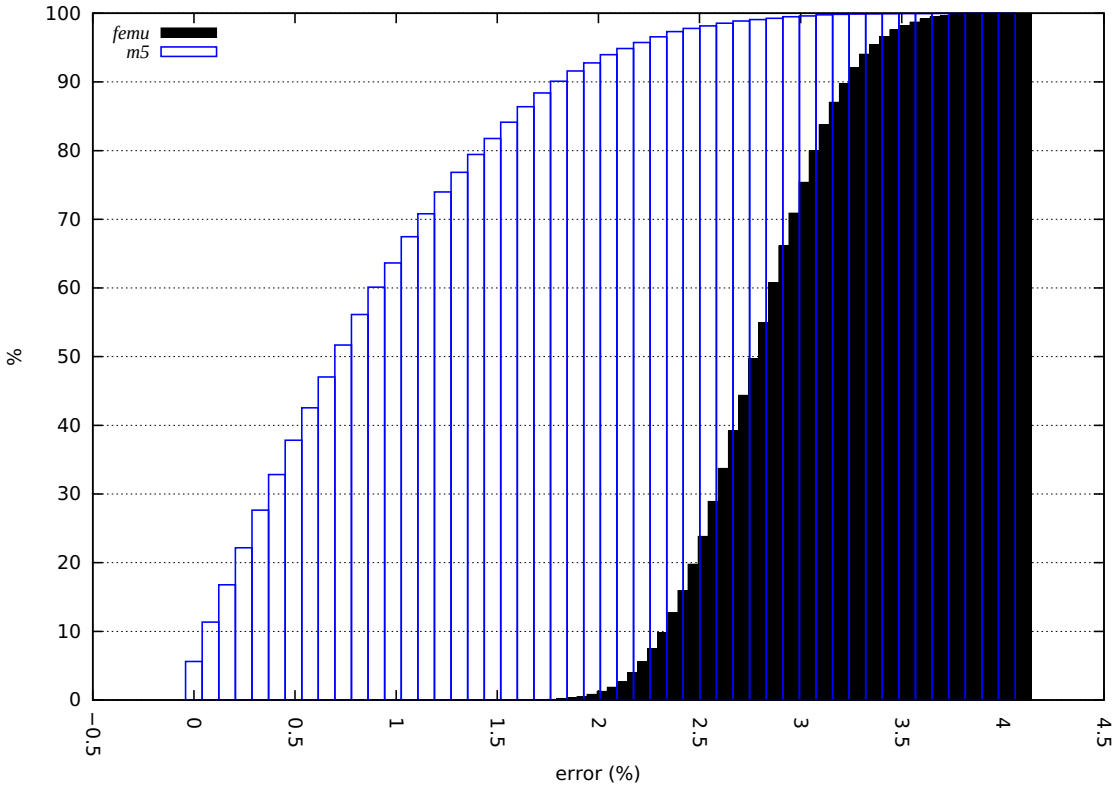

Figure 6: CDF of $\boldsymbol{e}_k$ using m5 (blue) and *femu* (black)

4.2. Second case study: 2D square

A square domain is submitted to uniformly distributed tractions $\boldsymbol{T}_d(t)$ on opposite horizontal edge as show in Figure 7. The length is $L = 0.01$ m. The loading evolution shape is unchanged from the previous study. $P_{max} = 16.0$ MPa, $t_1 = 0.1$ ms and $t_f = 0.25$ ms. The other boundary conditions are due to the symmetries of the considered problem. Indeed, in this case, we only study a quarter of the whole domain.

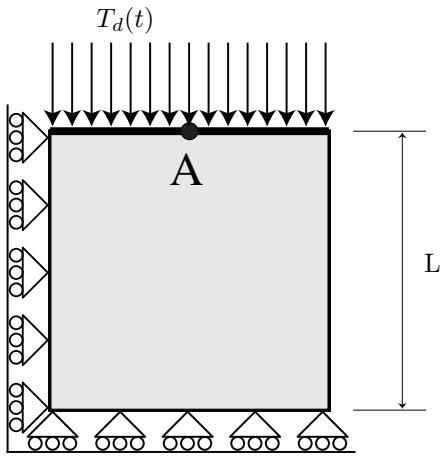

Figure 7: Test case 2 configuration

The matrix of noisy displacement $\mathbb{U}^{meas}$ is built as described in Section 2. A refined FE resolution is performed using a 1024 TRI3 element mesh and a fine time step ($\Delta t = 10^{-8}$ s). Measurements are performed using exact values of parameters : $\lambda_{ex} = 40.4\ GPa$ and $\mu_{ex} = 26.9\ GPa$.

For calculations made during the identification process, $\mathbb{U}^{calc}$ is built using a coarse FE mesh with 16 TRI3 elements and a centered difference scheme with time step equal to 10^{-7} s in accordance with CFL conditions (see equation (20)). The number of recordings for the identification is $N_{meas} = 250$.

For illustration purpose, Figure 8 show respectively the fine mesh, used to construct the synthetic measurements, and the coarse mesh, used for the FEMU calculations.

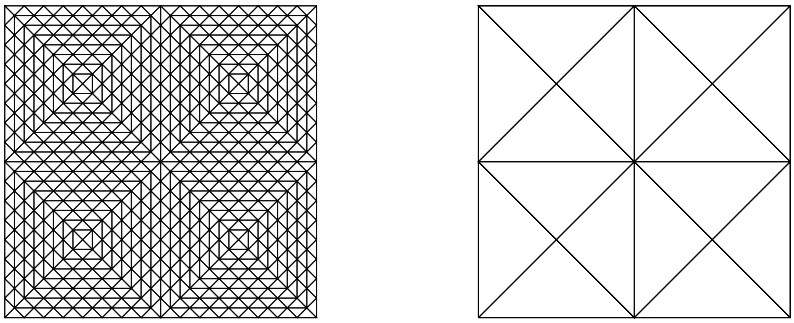

Figure 8: Illustration of the fine mesh ($N_{FE} = 1024$) and the coarse mesh ($N_{FE} = 16$)

Identification methods are listed in Table 3.

Table 3: Name of the identification methods used in our study

Name	Identification method
M1	$\boldsymbol{U}_2^*$ and $\boldsymbol{U}_1^* = \boldsymbol{U}(t,\omega)$ are used,
M2	$\boldsymbol{U}_2^*$ and $\boldsymbol{U}_1^* = \tilde{\boldsymbol{U}}(t,\omega)$(smoothing displacement) are used,
FEMU	the cost function $C_{\mathbf{u}}$ is used.

The Lamé coefficients are simultaneously identified by the FEMU method and our proposed method. We first analyse the influence of the mesh used for the calculations made during the identification process with FEMU. To that end, we evaluate the behavior of the FEMU method without adding noise ($\alpha = 0\%$). Figures 9 and 10 show respectively the error $e_\lambda(\%)$ and $e_\mu(\%)$ for different values of N_{FE}.

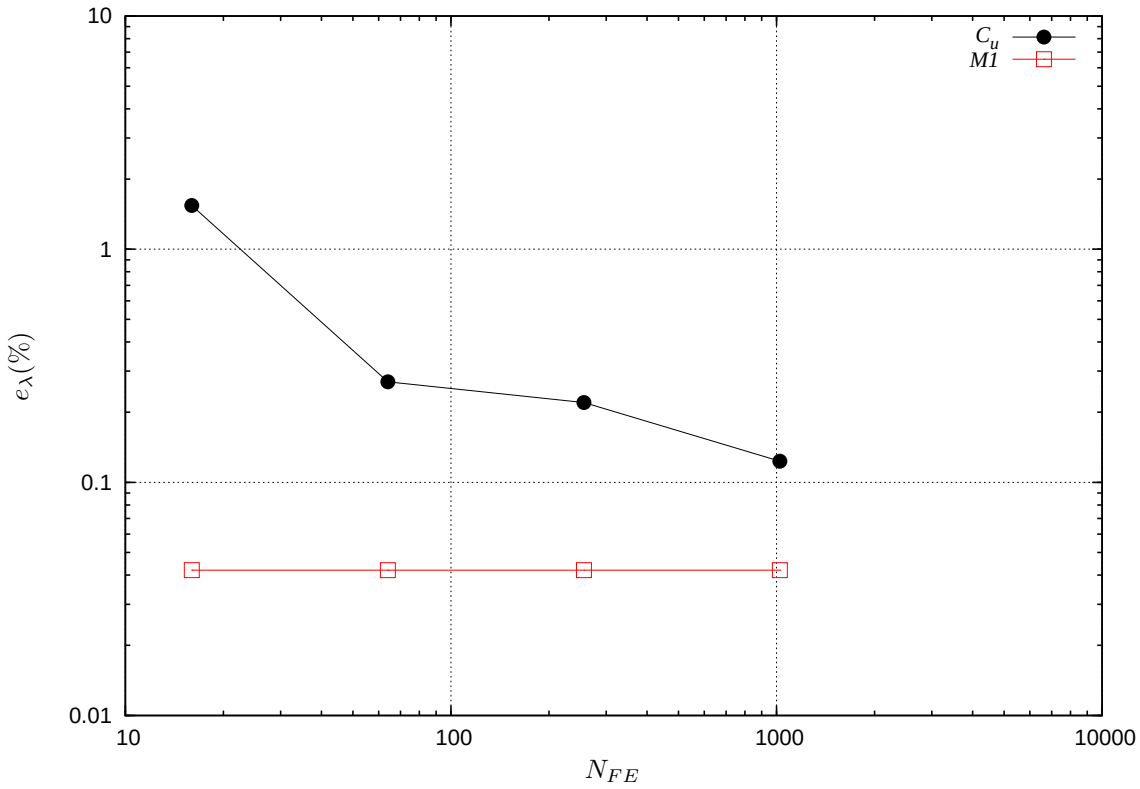

Figure 9: Error $e_\lambda(\%)$ for different values of N_{FE}

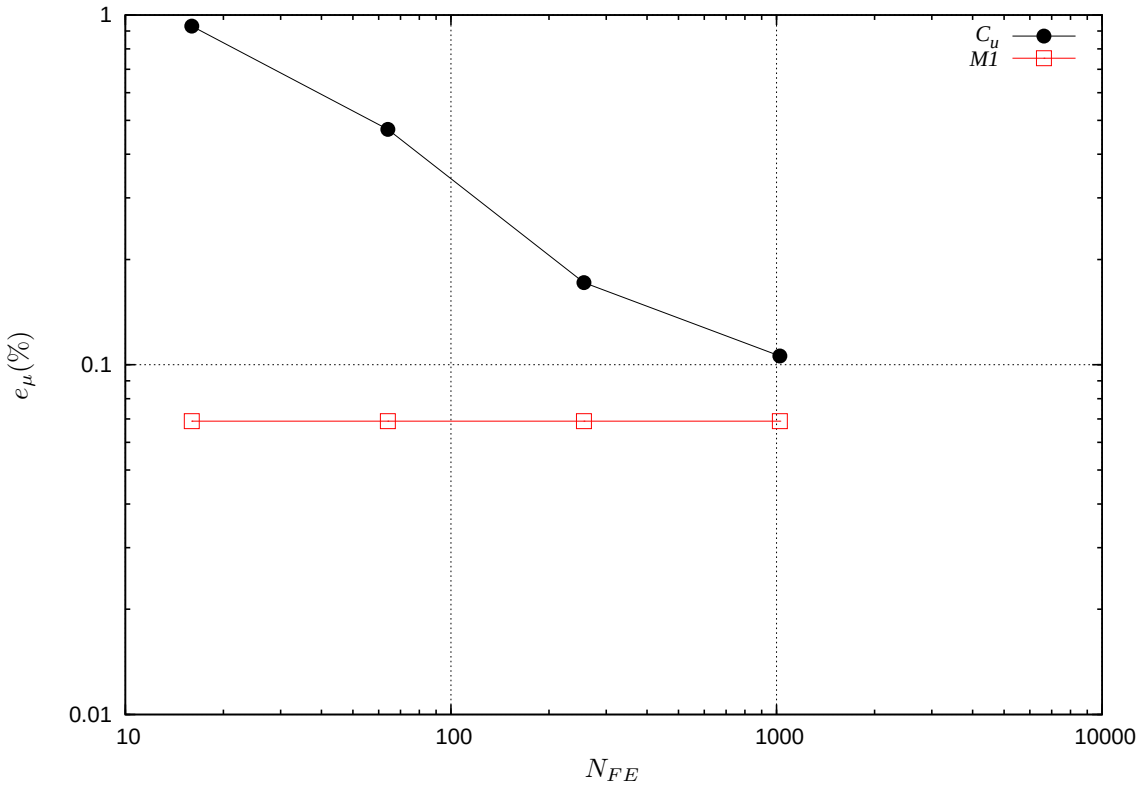

Figure 10: Error $e_\mu(\%)$ for different values of N_{FE}

For comparison purpose, the identification errors obtained with M1 are also given in the Figures 9 and 10. One can observe that better results are obtained with the proposed method denoted M1. The residual error observed when FEMU is performed with a very fine mesh ($N_{FE} = 1024$) is due to the difference between the integration schemes used for the exact measurement and the FEMU calculations. In the following we chose $N_{FE} = 16$ for FEMU, wich is seems a good balance between time consumption reasons and quality of the results (around $1\% error$).

In a second place, we analyse the behavior of the methods when noise on measurements is considered ($\alpha \neq 0$). Figures 11 (resp. 12) shows the error values $e_\lambda^{90\%}$ (resp. $e_\mu^{90\%}$) at $CDF(e_\lambda^{90\%}) = 90\%$ (resp. $CDF(e_\mu^{90\%}) = 90\%$) for different values of α.

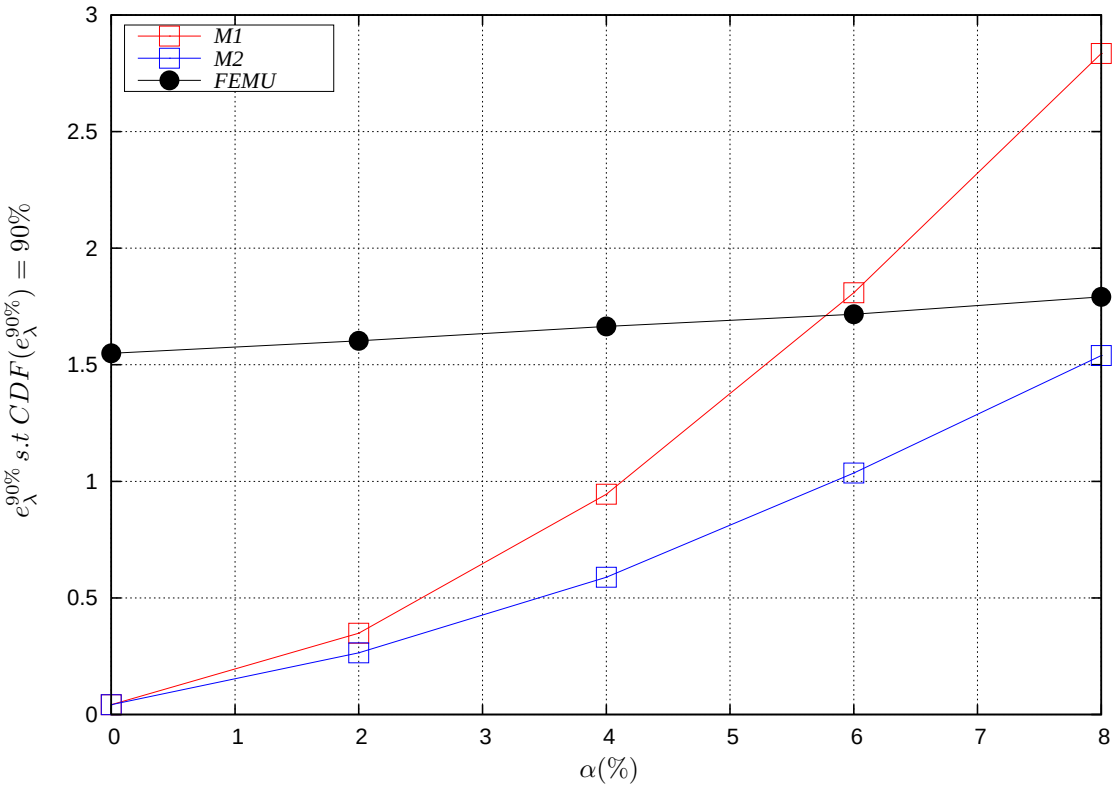

Figure 11: $e_\lambda^{90\%}\ s.t\ CDF(e_\lambda^{90\%}) = 90\%$ vs α

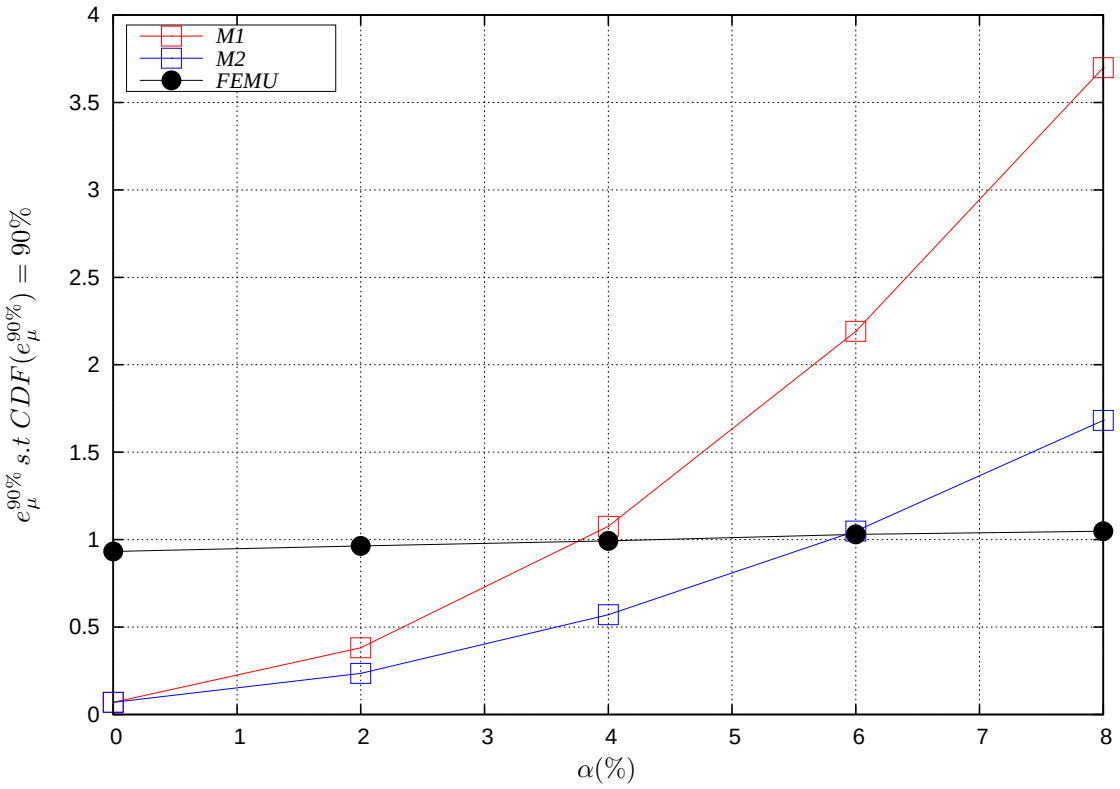

Figure 12: $e_\mu^{90\%}\ s.t\ CDF(e_\mu^{90\%}) = 90\%$ vs α

The mean variations ($\bar{e}_\lambda$, $\bar{e}_\mu$) and the standard deviations ($\hat{e}_\lambda$, $\hat{e}_\mu$) of the errors e_λ and e_μ are given in Table 4 for λ and Table 5 for μ.

Table 4: $\bar{e}_\lambda$ and $\hat{e}_\lambda$ vs α

	α	M1	M2	FEMU
	0%	0.042	0.042	1.55
	2%	0.20	0.14	1.55
$\bar{e}_\lambda(\%)$	4%	0.59	0.31	1.55
	6%	1.27	0.56	1.55
	8%	2.20	0.90	1.55
	0%	0.00	0.00	0.00
	2%	0.13	0.10	0.049
$\hat{e}_\lambda(\%)$	4%	0.29	0.22	0.098
	6%	0.45	0.37	0.15
	8%	0.60	0.54	0.20

Table 5: $\bar{e}_\mu$ and $\hat{e}_\mu$ vs α

	α	M1	M2	FEMU
$\bar{e}_\mu(\%)$	0%	0.069	0.069	0.93
	2%	0.27	0.14	0.93
	4%	0.89	0.37	0.93
	6%	1.90	0.76	0.93
	8%	3.31	1.30	0.93
$\hat{e}_\mu(\%)$	0%	0.00	0.00	0.00
	2%	0.090	0.081	0.026
	4%	0.18	0.17	0.053
	6%	0.27	0.27	0.079
	8%	0.36	0.36	0.10

Results show that the FEMU method is a robust identification procedure, similarly to what was observed in the previous case study (see section 4.1). In the present case study, the smoothing technique appears to be beneficial; it significantly improves our method without causing any important loss of mechanical information. The benefits of the smoothing technique for $\alpha = 8\%$ are shown in Figures 13 and 14 (for λ) and Figures 15 and 16 (for μ).

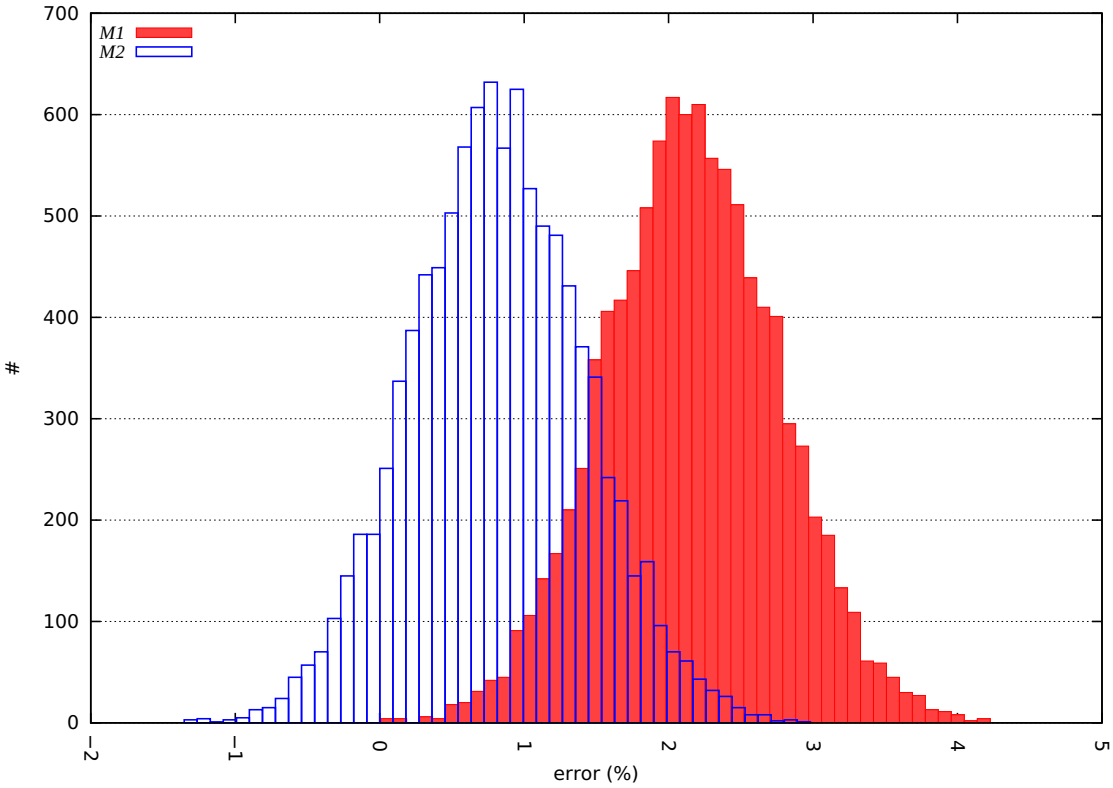

Figure 13: PDF of $\boldsymbol{e}_\lambda(\omega)$ using M1 (red) and M2 (blue)

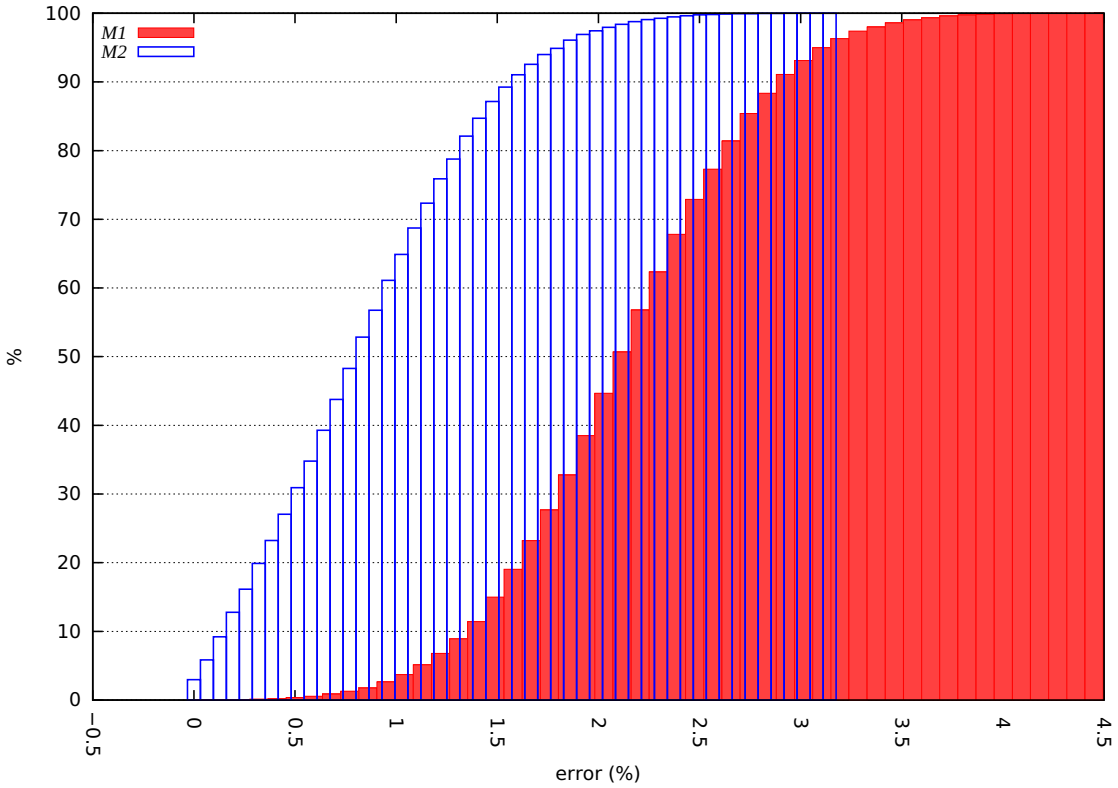

Figure 14: CDF of $\boldsymbol{e}_\lambda(\omega)$ using M1 (red) and M2 (blue)

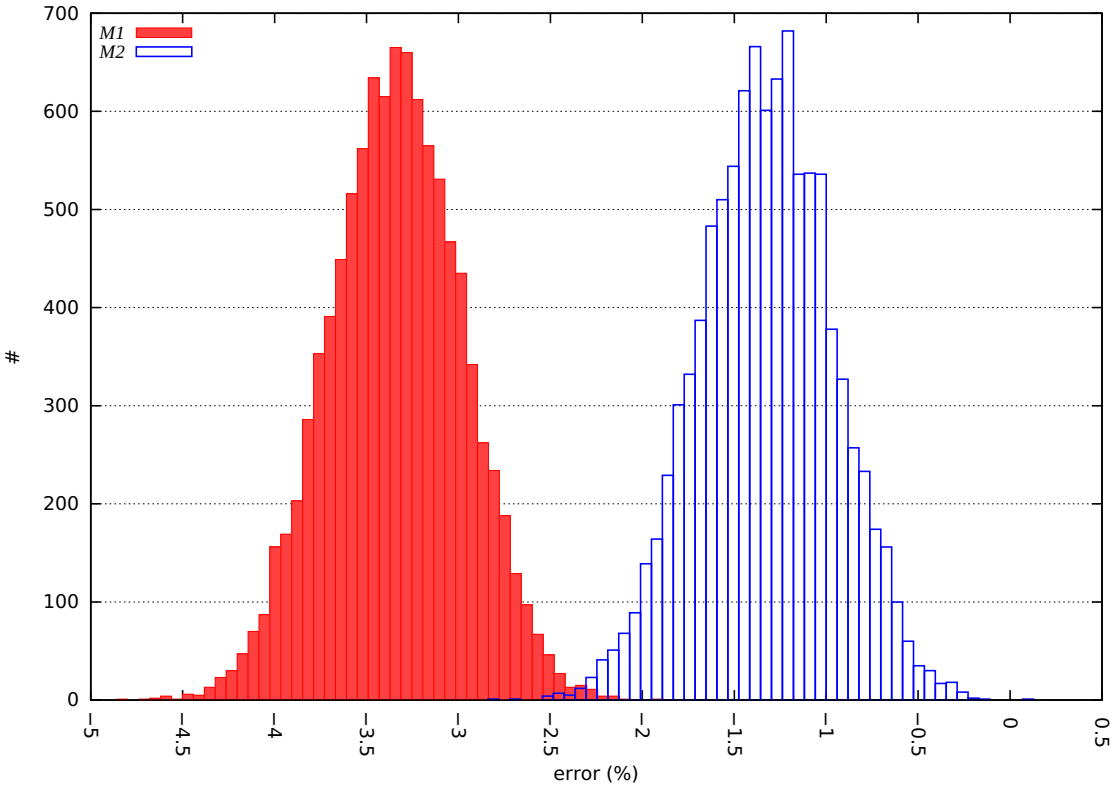

Figure 15: PDF of $\boldsymbol{e}_\mu(\omega)$ using M1 (red) and M2 (blue)

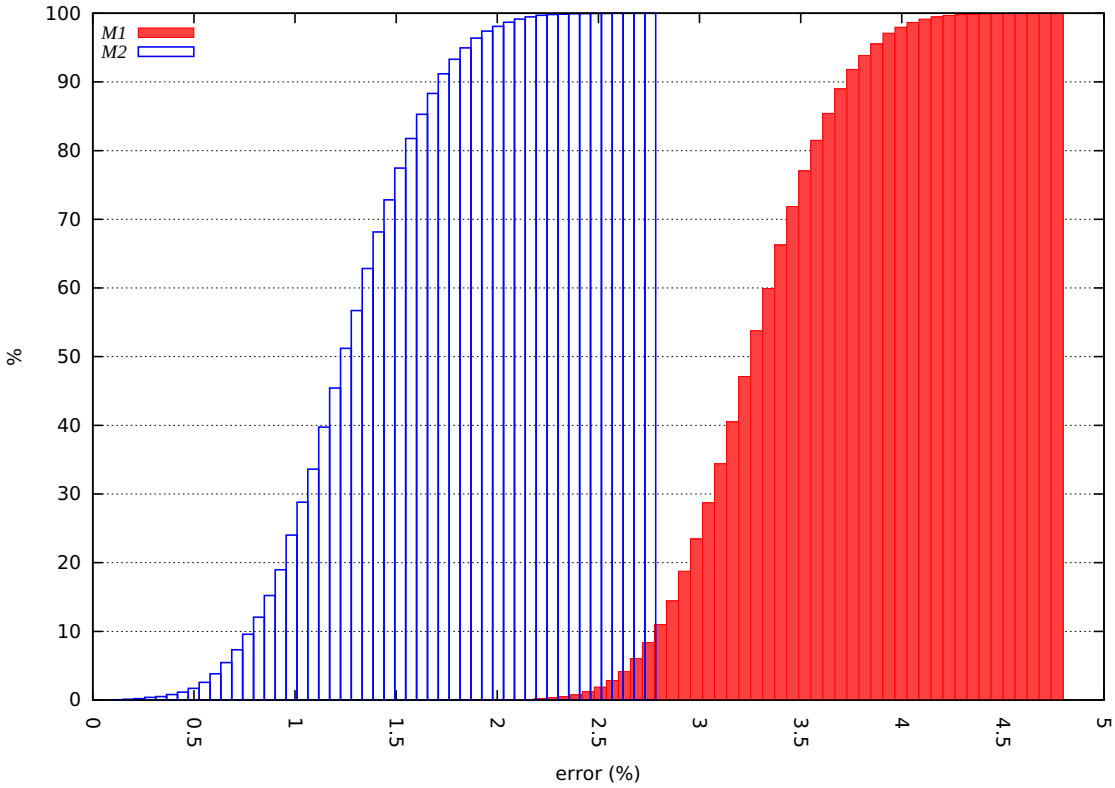

Figure 16: CDF of $\boldsymbol{e}_{\mu}(\omega)$ using M1 (red) and M2 (blue)

Based on Figures 13, 14, 15 and 16, we conclude that our proposed technique improves robustness and accuracy significantly. In Table 6, the CPU time for one identification is presented for the developed methods (M1 and M2) and is compared to the duration of one unique FE calculation.

Table 6: CPU time calculations for comparison

methods	time (ms)
M1	4.25
M2	4.32
FE	102.5

For accuracy purposes, all CPU times in Table 6 are based on 10 000 simulations. It is important to note that the smoothing technique is not time consuming. For example, one identification with M2 is 24 times less time-consuming than one FE simulation. In fact, the complete identification process is less time-consuming with our proposed methods than with the FEMU method. The absence of finite element iterations in our method is also an asset in transient dynamics. Indeed, FEMU identification requires at least one FE calculation.

4.3. Third case study: 2D square with a hole

The third case study differs from the previous one by its square hole at the center of the domain as shown in Figure 17. The loading evolution shape remains unchanged from previous studies. As for the previous case study, the boundary conditions are due to the symmetries of the considered problem. In this case, $P_{max} = 0.4$ MPa, $t_1 = 1.0$ ms and $2t_1 = t_f = 2.0$ ms and the lengths are $L = 0.1$ m and $l = 0.04$ m.

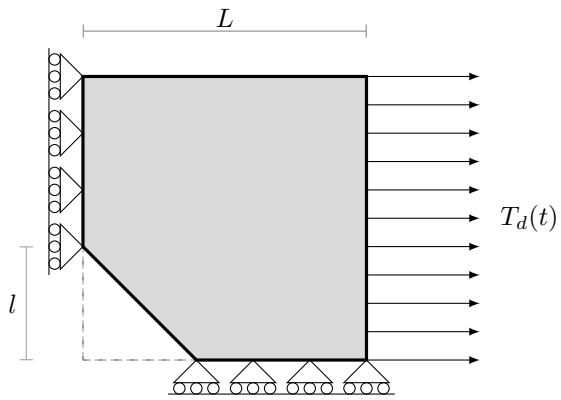

Figure 17: Test case 3 configuration

A refined FE resolution is performed with 1856 TRI3 elements and a fine time step: $\Delta t = 10^{-7}$ s. The measure is still obtained with the exact value of parameters : $\lambda_{ex} = 40.4$ GPa and $\mu_{ex} = 26.9$ GPa.

The calculations made during the identification process, $\mathbb{U}^{calc}$ are built using a coarse FE model with 29 TRI3 elements and a centered difference scheme time step equal to 10^{-7}s. This value is still chosen with respect to the CFL condition (see (20)). The number of recordings for the identification is $N_{meas} = 200$.

For illustration purpose, Figure 18 show respectively the fine mesh (used for generate synthetic data) and the coarse mesh (for FEMU identification) used in the following numerical examples.

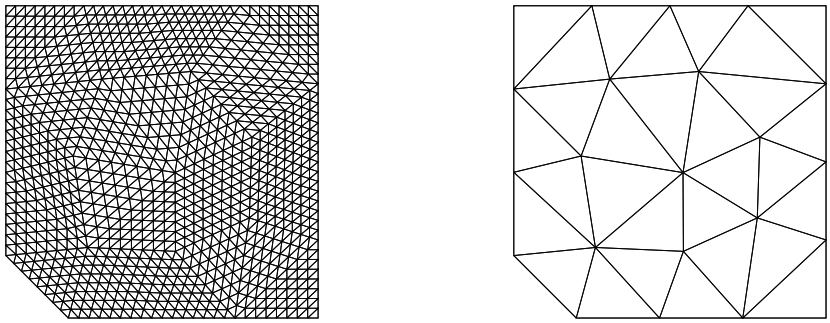

Figure 18: Illustration of the fine mesh ($N_{FE} = 1856$) and the coarse mesh ($N_{FE} = 29$)

Figures 19 and 20 represent the errors $e_{\lambda}^{90\%}$ and $e_{\mu}^{90\%}$ so that $CDF(e_{\lambda}^{90\%}) = 90\%$ and $CDF(e_{\mu}^{90\%}) = 90\%$ for different values of α.

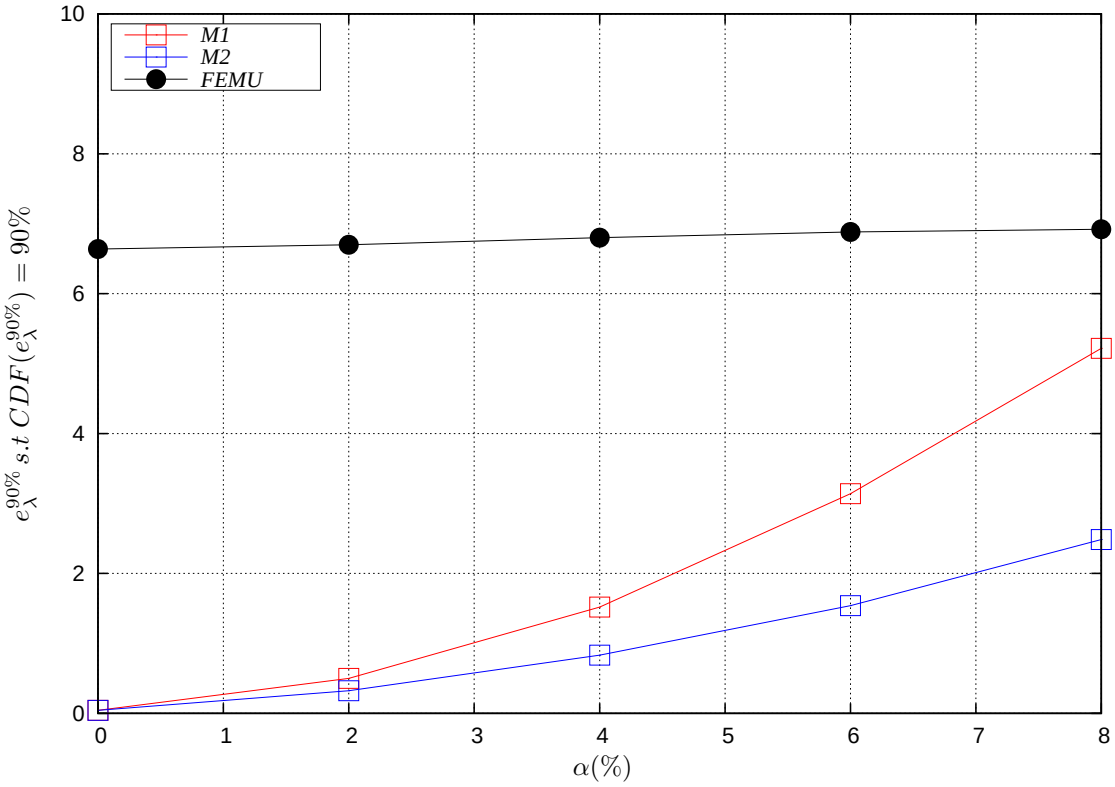

Figure 19: $e_{\lambda}^{90\%}\ s.t\ CDF(e_{\lambda}^{90\%}) = 90\%$ vs α

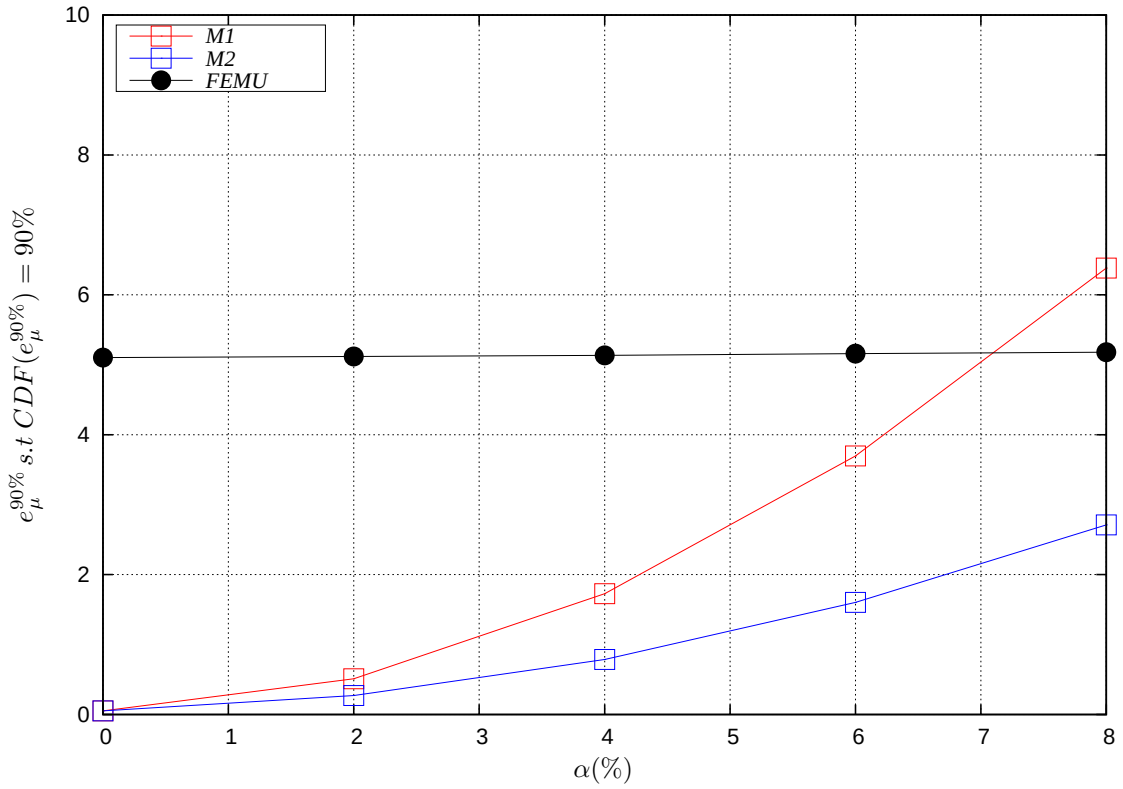

Figure 20: $e_\mu^{90\%}\ s.t\ CDF(e_\mu^{90\%}) = 90\%$vs α

The mean variations ($\bar{e}_\lambda$, $\bar{e}_\mu$) and standard deviations ($\hat{e}_\lambda$, $\hat{e}_\mu$) of the errors e_λ and e_μ are given in Table 7 for λ and Table 8 for μ.

Table 7: $\bar{e}_\lambda$ and $\hat{e}_\lambda$ vs α

	α	M1	M2	FEMU
$\bar{e}_\lambda(\%)$	0%	0.043	0.043	6.63
	2%	0.33	0.17	6.63
	4%	1.19	0.50	6.63
	6%	2.62	1.05	6.63
	8%	4.58	1.82	6.64
$\hat{e}_\lambda(\%)$	0%	0.00	0.00	0.00
	2%	0.15	0.12	0.07
	4%	0.30	0.27	0.13
	6%	0.45	0.44	0.20
	8%	0.61	0.60	0.25

Table 8: $\bar{e}_\mu$ and $\hat{e}_\mu$ vs α

	α	M1	M2	FEMU
$\bar{e}_\mu(\%)$	0%	0.052	0.052	5.10
	2%	0.43	0.19	5.10
	4%	1.57	0.63	5.10
	6%	3.45	1.37	5.10
	8%	6.02	2.40	5.10
$\hat{e}_\mu(\%)$	0%	0.00	0.00	0.00
	2%	0.072	0.072	0.01
	4%	0.14	0.14	0.02
	6%	0.22	0.22	0.049
	8%	0.31	0.29	0.065

Results are consistent with those obtained with a no-hole 2D square and show that our proposed method increases robustness. The smoothing technique also appears to be very beneficial.

4.4. Influence of the material

In this third case study (2D square with a hole) we identify the Lamé coefficients of an aluminum-like material. We now test the robustness of the proposed method, for the same case study, but with a different type of material. We perform numerical investigations to illustrate the influence of the material properties on our proposed method. Table 9 gives an overview of the standard elastic properties for different types of material.

Table 9: Standard values of parameters reflecting elastic properties of materials

	Steel	Aluminum	Glass	Wood	Concrete	Diamond
E(GPa)	210	70	60	7	35	1000
ν	0.285	0.3	0.25	0.2	0.2	0.1
$\rho(kg.m^{-3})$	7800	2700	2800	400	2400	3517
λ(GPa)	108.3	40.4	24	1.9	9.7	113.6
μ (GPa)	81.7	26.9	24	2.9	14.6	454.5

Tests are performed similarly to those conducted for an aluminum-type material (section 4.3) with $\alpha = 0\%$. In doing so, we only consider the deterministic part of the study.

Table 10 shows the relative identification errors e_λ and e_μ obtained for each material listed in Table 9.

Table 10: Quality of identification *vs.* material type, for both M2 and FEMU methods, with and without smoothing technique

		Steel	Aluminum	Glass	Wood	Concrete	Diamond
$e_\lambda(\%)$	M2	0.032	0.043	0.11	0.11	0.22	0.12
	FEMU	5.09	6.63	2.56	1.65	1.72	9.15
$e_\mu(\%)$	M2	0.028	0.052	0.056	0.047	0.077	0.027
	FEMU	6.12	5.10	6.62	7.23	3.91	5.61

We observe that, when a smoothing technique is used, the proposed method leads to better results for both parameters.

4.5. Loading uncertainties consideration

Previous studies only take into consideration the noise on measurements. However, during the measuring process of the displacement field (for instance by a DIC during a tensile test), the loading sensor can also lead to uncertainties as well as the CCD sensor. Here, we assess the behavior of the proposed method when noise on measurements and uncertainties on the loading evolution are taken into account simultaneously. To this end, we consider a random perturbation on the loading duration t_1 and on the loading intensity P_{max}. The evolution of the loading does not change (see Figure 3) but the loading duration becomes a random variable $\tilde{t}_1(\omega)$:

$$\tilde{t}_1(\omega) = \left(1.0 + \beta\,\psi_1(\omega)\right)\, t_1 \tag{58}$$

where ψ_1 is a centered uniform random variable with values within [-1,1] and β is a coefficient with values within $[0\%; 2\%; 4\%; 6\%; 8\%]$. By doing so, the mean of $\bar{t}_1$ is t_1.

The loading intensity also becomes a random variable $\tilde{P}_{max}$:

$$\tilde{P}_{max}(\omega) = \left(1.0 + \beta\,\psi_2(\omega)\right)\, P_{max} \tag{59}$$

where ψ_2 is also a centered uniform random variable with values within [-1,1].

Based on these considerations, new numerical investigations, illustrated on the third case study, are carried out to provide an assessment of the method (M2). Results are presented in Figures 21 and 22 for error values $e_\lambda^{90\%}$ and $e_\mu^{90\%}$ so that $CDF(e_\lambda^{90\%}) = 90\%$ and $CDF(e_\mu^{90\%}) = 90\%$ at different values of α and β.

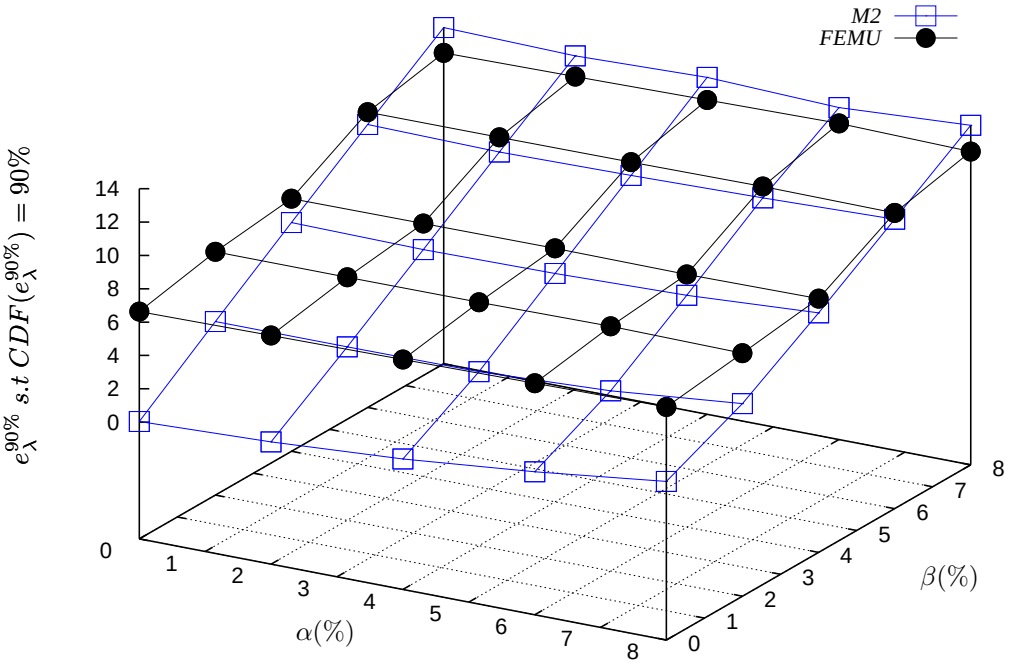

Figure 21: $e_\lambda^{90\%}$ $s.t\, CDF(e_\lambda^{90\%}) = 90\%$ vs α and β

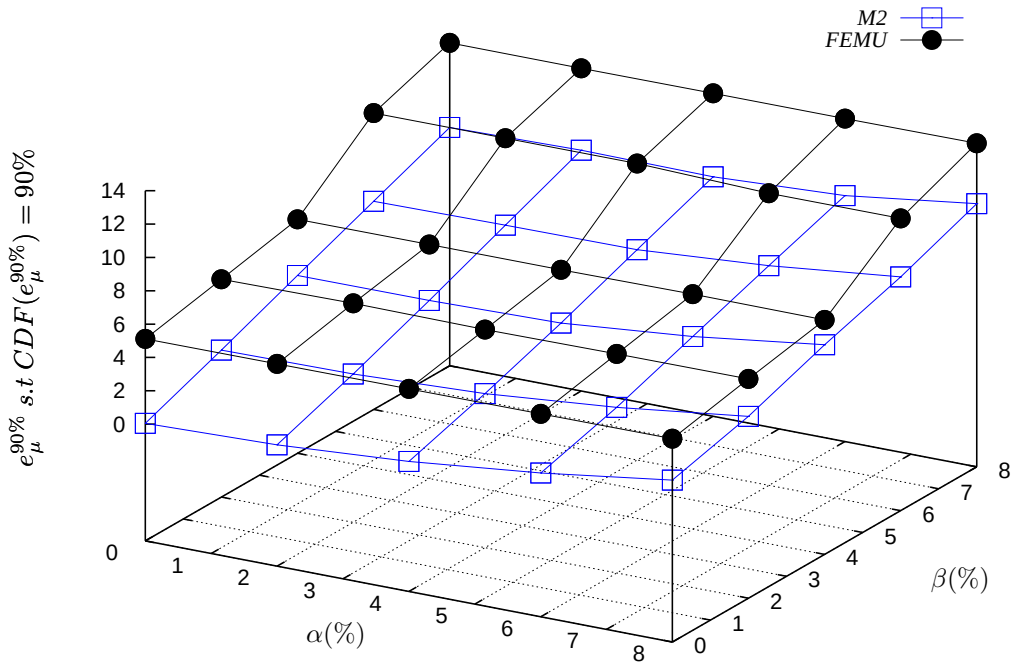

Figure 22: $e_\mu^{90\%}$ $s.t\, CDF(e_\mu^{90\%}) = 90\%$ vs α and β

We show that the uncertainties on the loading are more likely to deteriorate the behaviour performance of the proposed method (M2) than noise does on measurements. The robustness of the FEMU method is still observed but our new strategy leads to better results until $(\alpha, \beta) = 6\%$ which is an acceptable noise level for linear elasticity [3].

Similarly to previous observations made in the third case study, results are improved with the use of a smoothing technique on the virtual fields, without any significant loss of mechanical information.

4.6. Illustration of extension to multi-material

In this last case study, we illustrate one of the possible extensions of the proposed method (such as described in 3.2). Let us consider a multi-materials body as show in Figure 23.

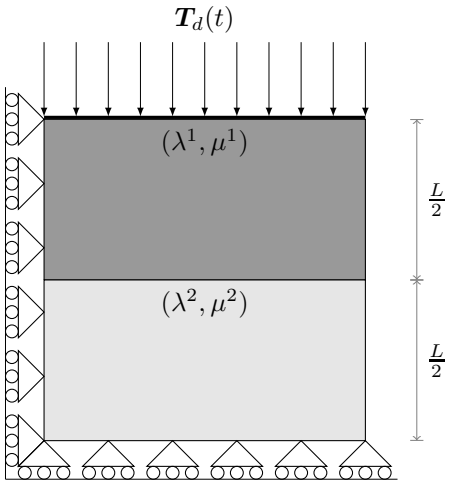

Figure 23: Forth case study

The domain initially used for the second case study is now split into two equal parts. The first half is represented by an isotropic elastic material with $\lambda^1_{ex} = 40\,GPa$ and $\mu^1_{ex} = 26\,GPa$. The second half is represented by an isotropic elastic material with $\lambda^2_{ex} = 80\,GPa$ and $\mu^2_{ex} = 52\,GPa$. Both parts are perfectly assembled.

The loading remains unchanged from the previous studies, the numerical values are: $P_{max} = 16.0$ MPa, $t_1 = 0.1$ ms and $t_f = 0.25$ ms. Other boundary conditions are symmetries. The length is $L = 0.01m$ and the number of recording for identification is $N_{mes} = 250$.

In order to have reliable synthetic data, we construct the reference data with a $N_{FE} = 2048$ mesh and the calculated data (for FEMU) with a $N_{FE} = 32$ mesh.

In this final case, we are interested in the identification of the 4 parameters: $\boldsymbol{\theta} = (\lambda^1, \mu^1, \lambda^2, \mu^2)$.

According to the developed strategy, one must chose 4 virtual fields in order to construct a small linear system. The following virtual fields are selected:

$$\boldsymbol{U}^*_1 = \boldsymbol{U}(t, \omega)\,, \quad \boldsymbol{U}^*_{2,3} = t^0\mathbf{1} \quad \text{and} \quad \boldsymbol{U}^*_4 = t^1\mathbf{1} \tag{60}$$

The choice $\boldsymbol{U}^*_{2,3} = t^0\mathbf{1}$ can be divided into two virtual fields as follow:

$$\boldsymbol{U}^*_2 = \begin{cases} t^0\mathbf{1} & \text{if} \quad y < \frac{L}{2} \\ \mathbf{0} & \text{else} \end{cases}$$

$$\boldsymbol{U}^*_3 = \begin{cases} t^0\mathbf{1} & \text{if} \quad y \geq \frac{L}{2} \\ \mathbf{0} & \text{else} \end{cases}$$

where y_{node} is the vertical component of the position.

Table 11 show the relative identification errors (e_{λ^1}, e_{μ^1}, e_{λ^2} and e_{μ^2}) for $\alpha = 0\%$ and $\beta = 0\%$ (none of the introduced perturbation are considered).

Table 11: Quality of the identification for FEMU, M1 and M2 methods

Material parameters:		λ^1	μ^1	λ^2	μ^2
$e_{\theta_i}(\%)$	FEMU	6.11	1.88	2.52	1.25
	M1	0.43	0.18	0.049	0.084
	M2	0.43	0.18	0.051	0.085

One can observe that the proposed method lead to better results. Furthermore, the smoothing technique do not deteriorate the quality of the identification as previously observed for the previous cases.

In the following, we assess the robustness of the methods M1 and M2 when noise on measurements is considered. Table 12 show the mean variations ($\bar{e}_{\lambda^1}$,$\bar{e}_{\mu^1}$,$\bar{e}_{\lambda^2}$,$\bar{e}_{\mu^2}$), the standard deviations ($\hat{e}_{\lambda^1}$,$\hat{e}_{\mu^1}$,$\hat{e}_{\lambda^2}$,$\hat{e}_{\mu^2}$) and the errors ($e^{90\%}_{\lambda^1}$,$e^{90\%}_{\mu^1}$,$e^{90\%}_{\lambda^2}$,$e^{90\%}_{\mu^2}$) for $\alpha = 8\%$ and $\beta = 0\%$.

Table 12: Accuracy and robustness of the proposed method (M1 and M2)

Material parameters:		λ^1	μ^1	λ^2	μ^2
$\bar{e}_{\theta_i}(\%)$	M1	3.55	3.91	4.75	3.23
	M2	1.45	1.60	1.94	1.32
$\hat{e}_{\theta_i}(\%)$	M1	2.06	2.26	2.75	1.86
	M2	2.01	2.24	2.73	1.86
$e^{90\%}_{\theta_i}(\%)$	M1	6.20	6.85	8.30	5.60
	M2	2.54	2.80	3.80	2.29

The comparison with the FEMU method is not available for this case study. Indeed, the identification of the four parameters is too long, due to the choice of a simple minimization based on dichotomy algorithm.

The observed conclusions are in agreement with the previous cases. Indeed, a reasonable noise level (8%) conduce to an error ($e^{90\%}_{\theta_i}$) lower than 4% when M2 is used. The use of a smoothing technique slightly improve (or does not change) the robustness of the method. Nevertheless, the mean variations and the errors ($e^{90\%}_{\theta_i}$) are significantly improved.

5. Conclusions

In our study, we propose a new identification method for extracting elastic properties of materials in transient dynamics. The method is based on the discrete finite element formulation from which a linear system is created by using a set of virtual fields in the time dimension. Our new method is less time-consuming than the FEMU method which is used as a reference for evaluation purposes. In fact, a significant advantage of the developed method is the direct identification process that allows to extract the parameters directly. For instance, current methods such as FEMU or CEGM are indirect and require an iterative minimization procedure.

The noise is one of the problems that can corrupt the data. This article is only based on numerical synthetic data. Therefore, the robustness of the developed approach has been studied numerically regarding noise on measurements and bad knowledge of the loading conditions.

Monte-Carlo simulations performed during numerical investigations, using synthetic data, demonstrate the accuracy and the robustness of this new method. A smoothing technique is also proposed in order to lower noise propagation; it appears to greatly improve the quality of the identification without causing any significant loss of mechanical information.

Other different problems can occur when using real data, for example misalignment between specimens and the acquisition system. In forthcoming work the method will be applied to real measurements in order to identify in a more realistic situation. This work is a first step of the development of the method. The proposed method seems adapted to the transient dynamics framework in linear elasticity. The proposed virtual fields are satisfying when a quasi-perfect framework is considered. The next step is to confront the developed method to a more complex situation. In the future, it would be also interesting to investigate new identification methods for large transformations and other non-linear real cases.

References

[1] Alfano M, Lubineau G, Paulino GH (2015) Global sensitivity analysis in the identification of cohesive models using full-field kinematic data. International Journal of Solids and Structures 55:66–78

[2] Avril S, Bonnet M, Bretelle AS, Grédiac M, Hild F, Ienny P, Latourte F, Lemosse D, Pagano S, Pagnacco E, Pierron F (2008) Overview of identification methods of mechanical parameters based on full-field measurements. Experimental Mechanics 48(4):381–402

[3] Ben Azzouna M, Feissel P, Villon P (2013) Identification of elastic properties from full-field measurements: a numerical study of the effect of filtering on the identification results. Measurement Science and Technology 24(5):055,603, URL http://stacks.iop.org/0957-0233/24/i=5/a=055603

[4] Blaysat B, Grédiac M, Sur F (2016) On the propagation of camera sensor noise to displacement maps obtained by dic - an experimental study. Experimental Mechanics 56(6):919–944, DOI 10.1007/s11340-016-0130-9, URL https://doi.org/10.1007/s11340-016-0130-9

[5] Bonnet M, Constantinescu A (2005) Inverse problems in elasticity. Inverse Problems 21(2):R1, URL http://stacks.iop.org/0266-5611/21/i=2/a=R01

[6] Bui HD, Constantinescu A, Maigre H (2004) Numerical identification of linear cracks in 2d elastodynamics using the instantaneous reciprocity gap. Inverse Problems 20(4):993, URL http://stacks.iop.org/0266-5611/20/i=4/a=001

[7] Chu TC, Ranson WF, Sutton MA (1985) Applications of digital-image-correlation techniques to experimental mechanics. Experimental Mechanics 25(3):232–244, DOI 10.1007/BF02325092, URL http://dx.doi.org/10.1007/BF02325092

[8] Claire D, Hild F, Roux S (2004) A finite element formulation to identify damage fields: The equilibrium gap method. International Journal of Numerical Methods in Engineering 62:189–208, DOI 10.1002/nme.1057, URL https://hal.archives-ouvertes.fr/hal-00002899

[9] Erdogan YS, Catbas FN, Bakir PG (2014) Structural identification (st-id) using finite element models for optimum sensor configuration and uncertainty quantification. Finite Elements in Analysis and Design 81:1 – 13, DOI http://dx.doi.org/10.1016/j.finel.2013.10.009, URL http://www.sciencedirect.com/science/article/pii/S0168874X13001765

[10] Faverjon B, Puig B, Baranger T (2017) Identification of boundary conditions by solving cauchy problem in linear elasticity with material uncertainties. Computers and Mathematics with Applications 73(3):494 – 504, DOI https://doi.org/10.1016/j.camwa.2016.12.011, URL http://www.sciencedirect.com/science/article/pii/S0898122116306824

[11] Feissel P, Allix O (2007) Modified constitutive relation error identification strategy for transient dynamics with corrupted data: The elastic case. Computer Methods in Applied Mechanics and Engineering 196(13-16):1968 – 1983, DOI http://dx.doi.org/10.1016/j.cma.2006.10.005, URL http://www.sciencedirect.com/science/article/pii/S0045782506003434

[12] Florentin E, Lubineau G (2010) Identification of the parameters of an elastic material model using the constitutive equation gap method. Computational Mechanics 46(4):521–531, DOI 10.1007/s00466-010-0496-y, URL http://dx.doi.org/10.1007/s00466-010-0496-y

[13] Grédiac M, Toussaint E, Pierron F (2002) Special virtual fields for the direct determination of material parameters with the virtual fields method. 1-principle and definition. International Journal of

Solids and Structures 39(10):2691 – 2705, DOI http://dx.doi.org/10.1016/S0020-7683(02)00127-0, URL http://www.sciencedirect.com/science/article/pii/S0020768302001270

[14] Grédiac M, Pierron F, Avril S, Toussaint E (2006) The virtual fields method for extracting constitutive parameters from full-field measurements: a review. Strain 42(4):233–253

[15] Kavanagh KT, Clough RW (1971) Finite element applications in the characterization of elastic solids. International Journal of Solids and Structures 7(1):11–23, DOI http://dx.doi.org/10.1016/0020-7683(71)90015-1

[16] Passieux JC, Bugarin F, David C, Périé JN, Robert L (2015) Multiscale displacement field measurement using digital image correlation: Application to the identification of elastic properties. Experimental Mechanics 55(1):121–137, DOI 10.1007/s11340-014-9872-4, URL http://dx.doi.org/10.1007/s11340-014-9872-4

[17] Rosenzveig G, Louf F, Champaney L (2016) A fe model updating method for the simulation of the assembly process of large and lightweight aeronautical structures. Finite Elements in Analysis and Design 111:56–63

[18] Sutton M, Wolters W, Peters W, Ranson W, McNeill S (1983) Determination of displacements using an improved digital correlation method. Image and Vision Computing 1(3):133–139, DOI http://dx.doi.org/10.1016/0262-8856(83)90064-1

[19] Toussaint E, Grédiac M, Pierron F (2006) The virtual fields method with piecewise virtual fields. International Journal of Mechanical Sciences 48(3):256 – 264, DOI http://dx.doi.org/10.1016/j.ijmecsci.2005.10.002, URL http://www.sciencedirect.com/science/article/pii/S0020740305002419

[20] Touzeau C, Magnain B, Emile B, Laurent H, Florentin E (2016) Identification in transient dynamics using a geometry-based cost function in finite element model updating method. Finite Elements in Analysis and Design 122:49 – 60, DOI http://dx.doi.org/10.1016/j.finel.2016.09.003, URL //www.sciencedirect.com/science/article/pii/S0168874X16302918